Probing metazoan polyphosphate biology using *Drosophila* reveals novel and conserved polyP functions

Authors: Sunayana Sarkar[1], Harsha Sharma[1], SK Yasir Hosen[1], Jayashree S Ladke[2,5], Sandra Moser[3,4], Deepa Balasubramanian[1], Sreejith Raran-Kurussi[1], Henning Jessen[3,4], Rashna Bhandari[2,*], Manish Jaiswal[1,*]

[1] Tata Institute of Fundamental Research Hyderabad, Ranga Reddy Dist. Hyderabad, 500046, India.

[2] Centre for DNA Fingerprinting and Diagnostics, Inner Ring Road, Uppal, Hyderabad, 500039, India.

[3] Institute of Organic Chemistry, Albert-Ludwigs-Universität Freiburg, Albertstraße 21, 79104 Freiburg in Breisgau, Germany.

[4] CIBSS – Centre for Integrative Biological Signalling Studies, Albert-Ludwigs-Universität Freiburg, Schänzlestraße 18, 79104 Freiburg in Breisgau, Germany.

[5] Graduate Studies, Regional Centre for Biotechnology, Faridabad 121001, Haryana, India.

[*]Corresponding authors

Lead contact: manish@tifrh.res.in

Classification: Biological Sciences/Physiology

Key words: polyP Biology, Phosphate Metabolism, *Sc*PpX1, polyP detection, polyP depletion

Abstract

Polyphosphate (polyP) exists in all life forms; however, its biological functions in metazoans are understudied. Here, we explored *Drosophila,* to our knowledge, as the first genetic model to explore polyP biology in metazoans. We established biochemical and *in situ* methods to detect, quantify, and visualise polyP in *Drosophila.* We then engineered a FLYX system to deplete polyP in subcellular compartments in a tissue-specific manner. Using these tools, we demonstrated a spatiotemporal and subcellular compartment-specific regulation of polyP levels in various developmental stages and tissue types. We discovered that polyP is crucial for *Drosophila* hemolymph clotting and proper developmental timing, consistent with an evolutionarily conserved role as exogenous polyP also accelerates mammalian blood clotting. Further, the transcriptomics analysis of polyP-depleted larvae demonstrates the impact of polyP on several cellular processes, including translation. These observations underscore the utility of the toolkit we developed to discover previously unknown polyP functions in metazoans.

Introduction:

Inorganic polyphosphate (polyP), a linear polymer of variable chain lengths of orthophosphate (Pi) moieties linked via phosphoanhydride bonds, was first observed in the bacteria *Spirillum volutans* and was termed as volutin granules (1,2). Arthur Kornberg's works showed that polyP is present in archaea, eubacteria and mammals (3,4). Our current understanding of the biological functions and the molecular mechanisms of polyP predominantly stems from studies in prokaryotes and a few single-cell eukaryotes (e.g., *Saccharomyces cerevisiae*, *Schizosaccharomyces pombe* and *Dictyostelium sp*.). In bacteria, polyP is shown to serve as a phosphate reservoir, aid in biofilm formation, and help in transposon silencing (5–7). In algae, polyP acts as an antioxidant, metal chelator, and buffer against alkaline stresses (3,8–10). However, in metazoans, the biological functions of polyP have been underexplored, and thus, it used to be referred to as a molecular fossil.

Ex vivo and *in vitro* works in mammals have suggested the implications of polyP in blood coagulation, mitochondrial function, bone mineralisation, and neuronal activity (11–18). Moreover, recent works have discovered that several mammalian proteins, known to be involved in cellular processes such as transcription and translation, can bind to polyP. Binding to polyP may alter the localization, structure, or function of proteins, thereby affecting several biological processes in metazoans (19–21). Recent studies have also implicated polyP in human diseases, such as the pathogenesis of amyotrophic lateral sclerosis (ALS) (22). Further, a clinical trial has found beneficial effects of polyP in treating ulcerative colitis (23). Furthermore, feeding polyP to aβ-expressing *Caenorhabditis elegans* (Alzheimer's model) led to rescuing

paralytic behaviour (5). Thus, it is emerging that polyP is not a relic; it affects several physiological processes in metazoans, including human diseases.

Efficient tools for quantification and genetic manipulation of polyP in prokaryotic models and yeast have been crucial in exploring polyP biology. Discovery of PolyP kinases (PPK1 in bacteria, VTC4 in yeasts) and Polyphosphatases (PPN2 in bacteria, ScPPX in yeasts) - enzymes to synthesise and degrade polyP in prokaryotes and yeasts allowed phenotypic studies in these organisms (24–30). In contrast, our knowledge of polyP and its roles remains limited in multicellular eukaryotes. Although recent work has reported that the FoF1 complex of ATPase in the mitochondria is required for polyP synthesis, PolyP kinases and polyphosphatases in multicellular organisms remain unknown (31). Purified human Prune is shown to have a short-chain exopolyphosphatase activity *in vitro* (32). Recently, biochemical experiments led to the discovery of endopolyphosphatase NUDT3, an enzyme known as a dinucleoside phosphatase (33). The function of these proteins in regulating polyP has yet to be tested *in vivo* in a genetically tractable metazoan model.

A significant gap in studying polyP in multicellular eukaryotes is the lack of a genetic model system that allows sensitive methods for visualising, quantifying, and manipulating polyP. *Drosophila melanogaster* provides an ideal platform to close this gap: it combines powerful genetics with short generation time and well-characterized development, enabling systematic interrogation of polyP dynamics in vivo. However, methods for sensitive quantification, visualization, and genetic perturbation of polyP have not been established in flies or any other metazoan model. Here, we report a toolkit to quantify, visualise, and genetically manipulate

polyP levels in *Drosophila*. Using this toolkit, we show that polyP levels undergo temporally regulated fluctuations that can influence organismal development and physiology through possible evolutionarily conserved mechanisms. Overall, this work establishes *Drosophila* as a valuable *in vivo* model to dissect the functions of polyP in metazoans.

Results:

Development of methods for the extraction and quantification of polyP from flies

The polyP levels have been shown to vary among species. Bacteria like *E.coli* maintain as low as 100uM polyP (Pi terms) which surges to nearly 50mM in stress conditions; yeasts have been reported to have a polyP content of ~100mM (Pi terms) whereas in mammalian cells, polyP levels vary in low micromolar concentrations (~10–90uM polyP in Pi terms) (3). Since metazoans have lower polyP content, to use *Drosophila* as a model system, it was essential to re-standardise a method sensitive enough to extract and quantify polyP from fly samples. Various biochemical strategies for extracting polyP from biological samples have been discussed, each with its own limitations (34). The acid-based extraction method fails to preserve the entire chain length of polyP, as polyP is unstable in strongly acidic conditions. In contrast, column purification can only retain polyP of longer chain lengths (>60-80). PolyP extraction using saturated phenol (in citrate buffer pH 4.1) and chloroform, followed by ethanol precipitation, can efficiently pellet down polyP. However, this method also co-purifies RNA, which may interfere with polyP quantification. Thus, to extract polyP from *Drosophila* samples, we standardised the citrate-saturated phenol-chloroform-based method followed by RNase treatment **(Fig 1A, Supplementary Fig 1A, See Materials and Methods)**.

To quantify polyP levels, several techniques based on Nuclear Magnetic Resonance (NMR), chromatography, radioactive isotope labelling, and enzymatic digestion have been used (35). We used the enzymatic detection method to quantify polyP extracted from fly tissues, as it has higher specificity and sensitivity (36,37). This method involved the digestion of polyP by recombinant *S. cerevisiae* exopolyphosphatase 1 (*Sc*PpX1), followed by colorimetric measurement of the released Pi by malachite green. Malachite green and ammonium molybdate, when mixed in a 3:1 ratio, form a metachromatic brown-coloured adduct that turns green upon conjugation with monophosphate (38,39) and can be quantified based on absorbance at 650 nm. Therefore, absorbance measurements from *Sc*PpX1 digested polyP can be interpolated to quantify the Pi released from extracted polyP samples. Thus, the intensity of the green colour is a measure of the free Pi, which in turn is a measure of the polyP levels. This assay allows the measurement of polyP content indirectly in terms of the liberated Pi **(Supplementary Fig 1B, See Materials and Methods)**.

To standardise the polyP quantification method, we extracted polyP from fly larvae, and the extracted polyP was incubated with purified recombinant *Sc*PpX1 for 18 hours at 37°C to digest polyP completely. The other half was left untreated for 18 hours at 37°C. Malachite green was added to both samples, and the background from any preexisting Pi in the untreated sample was subtracted to quantify the Pi content. For calibration of the assay, increasing concentrations of KH_2PO_4 were used to draw a standard curve (37–39). The amount of recovered polyP was proportional to the number of larvae used for polyP extraction **(Fig 1B)**. The polyP content in each third instar larval was found to be 419.30 ± 36.83 picomoles in Pi terms **(Table 1),** and the normalised polyP level is 46.8 ± 3.95 picomoles polyP (Pi terms) per milligram protein from the third instar larval lysate **(Table 1)**.

PolyP levels are developmentally regulated

Given the various possible roles of polyP, we sought to test if polyP levels are developmentally regulated in *Drosophila*. First, we quantified polyP at every two-hour interval during the embryonic stages of development. As shown in **Fig 1C and Table 2**, we observed no significant change in polyP levels across various embryonic stages. We then compared polyP content at different stages of the *Drosophila* life cycle - embryos, larval stages (first instar, second instar, feeding third instar, non-feeding third instar, pupal stages (prepupae and one-day-old pupae), pharate adult, and three-days-old adults. The polyP content remains unchanged from embryos to the third instar feeding larval stages, followed by an increase in the third instar non-feeding larval stage. The polyP content reduces during metamorphosis and drops significantly in the pharate, the stage when the adults are ready to eclose from pupa, followed by a subtle increase in three-day-old flies **(Fig 1D, Table 3)**. These observations show a temporal regulation of polyP during development, and the increased polyP levels at the late third instar larval stages could constitute a phosphate reservoir for metamorphosis during pupal stages.

In-situ labelling of polyP in *Drosophila* tissues revealed spatiotemporal polyP dynamics

To investigate the subcellular localization of polyP across different tissue types, we developed an *in situ* label of polyP using the PolyP Binding Domain (PPBD) of the *E.coli* exopolyphosphatase PPX. PPBD was initially shown to specifically bind polyP *in vitro* with a high affinity of ~45μM for longer polyP chains (35 mer and above), and it can detect polyP localized in budding yeast vacuoles, mammalian mast cell granules, and *C.elegans* (40,41)

(41–43). Thus, in this study, we used recombinant GST-PPBD protein to label polyP in fly tissues **(Fig 2A, Materials and Methods)**.

To standardise the labelling method, we determined a tissue fixation method and tested methanol, 4% paraformaldehyde and Bouin's fixatives and found that 4% paraformaldehyde works better among the three for labeling polyP in fly tissues **(Supplementary Fig 2A)**. To test the specificity of GST-PPBD, we used a mutant PPBD (GST-PPBD^{Mut}) and GST proteins. To create GST-PPBD^{Mut} we replaced eight basic amino acid residues with Alanine **(Fig 2B, See Material and Methods for sequence)**. These amino acids were selected based on structural studies of *E. coli* PPX that contains PPBD domain (27,30). The predicted structure of the PPBD^{Mut} aligned with PPBD and had a r.m.s.d. value of 0.024 suggesting no major change in structure of the protein **(Fig 2B)**. We synthesized diamine-linked polydisperse PolyP$_{100}$ and labelled both the ends with Fluorescein Isothiocyanate (FITC) to yield Bis-FITC-labeled PolyP$_{100}$ (PolyP$_{100}$-2X-FITC) following a synthetic procedure described by Fernandes-Cunha et al. (44) **(See Supplementary Supplementary Text for Materials and Methods)**. Using Microscale Thermophoresis (MST), we found that GST-PPBD binds to PolyP$_{100}$-2X-FITC whereas GST-PPBD^{Mut} and GST do not show binding to PolyP$_{100}$-2X-FITC **(Fig 2C, See Material and Methods)**. We then performed immunofluorescence experiments with GST, GST-PPBD, and GST-PPBD^{Mut} on hemocytes and found that unlike GST-PPBD, GST-PPBD^{Mut} or GST protein does not show any specific staining pattern **(Fig 2D)**. Thus, GST-PPBD^{Mut} and GST protein can serve as checkpoints for the specificity of GST-PPBD based labeling of polyP. To further test the specificity, we treated fixed and permeabilised hemocytes with *Sc*PpX1 and heat inactivated *Sc*PpX1 for 2 hours at 37℃ and found that both the staining intensity and the

number of PPBD punctae were reduced in hemocytes treated with active *Sc*PpX1, as compared to untreated control and heat inactivated *Sc*PpX1 **(Fig 2E-G,** method adopted from Quarles et. al (43)**)**.

We systematically analysed GST-PPBD labelling in several fly tissues and observed distinct patterns in different tissue types **(Fig 3 and Supplementary Fig 3)**. We observed GST-PPBD labelling in cytoplasmic puncta, nuclear compartments, or both in a tissue-specific manner **(Fig 3 and Supplementary Fig 3)**. In cells with larger nuclei, *e.g.* in salivary glands, we observed intense GST-PPBD labelling in subnuclear compartments devoid of DAPI staining **(Fig 3A ii, iv)**. We suspected these compartments to be nucleoli. To test this, we co-stained GST-PPBD with an antibody against fibrillarin, a nucleolar protein, and found colocalization of these proteins, suggesting that polyP is enriched in the nucleolus **(Fig 3B-C)**. This is consistent with recent reports which found that polyP binds to nucleolar proteins (45,46). Further, in wing and eye larval imaginal discs we found punctate cytoplasmic and nucleolar labelling of GST-PPBD. However, leg and haltere imaginal discs showed no difference in GST-PPBD staining compared to the GST control. In contrast, the larval crop and muscle showed nucleolar GST-PPBD with an intense cytoplasmic background **(Supplementary Fig 3)**.

Interestingly, GST-PPBD labelling revealed spatial and temporal dynamics of polyP localisation during oogenesis. We observed intense GST-PPBD labelling in the nucleus and cytoplasm of the nurse and follicle cells in the early stages of ovary development **(Fig 3D)**. However, there is a gradual reduction in the intensity of GST-PPBD labelling from stage S2 to S9 ovaries, indicating a gradual decrease in polyP levels, indicating the potential stage-specific

physiological role of polyP **(Fig 3D)**. Earlier reports have also demonstrated polyP localization in the zona pellucida of mice ovaries and in cockroach oocytes indicating a possible role of polyP during oogenesis (47–49). In hemocytes (hemolymph cells, equivalent to mammalian blood cells) we found an intense GST-PPBD labelling exhibiting polyP localization in large granular structures close to the periphery **(Fig 3E-H)**. The hemocytes were identified by the expression of GFP reporters, driven by cell-specific promoters of *hemolectin* (*hml-GAL4>UAS-GFP*) in plasmatocytes and *lozenge* (*lz-GAL4>UAS-mCD8::GFP*) in crystal cells. Overall, to our knowledge, this is the first comprehensive tissue staining report exhibiting the spatiotemporal dynamics of polyP within a multicellular organism. Taken together, these data also indicate tissue-specific regulation and biological function of polyP in metazoans.

A heterologous system to deplete polyP in flies: FLYX- Fly expressing *Sc*PpX1

Since metazoan polyP kinases and polyphosphatases are still elusive, direct genetic manipulation of polyP levels can not be done to probe its function in flies. Heterologous expression of budding yeast exopolyphosphatase enzyme (*Sc*PpX1) can deplete polyP in mammalian cells (50). Therefore, to investigate the biological function of polyP, we developed transgenic fly lines that allow tissue-specific and subcellular depletion of polyP by heterologous expression of *ScPpX1*. These flies that will express *Sc*PpX1 constitute the 'FLYX' system.

To develop the FLYX system, we codon optimised and synthesised N-terminal HA-tagged *ScPpX1* (HA-*ScPpX1*) (material and methods for sequence). For the tissue-specific expression of HA-*Sc*PpX1 in the FLYX system, we used the UAS-GAL4 system (51,52). The transcription activator GAL4 is expressed under a tissue-specific promoter in this system. When GAL4 binds to the upstream activator sequence (UAS) preceding the cDNA sequence of interest, the protein

is expressed in the specific tissue**,** thereby providing a handle for spatial regulation of polyP **(Fig 4A-B)**. We cloned codon-optimised HA-*ScPpX1* into fly transgenesis vector pUAST-AttB and pUASp, which allows site-specific integration of a construct in the fly genome via φC31 Integrase system (53). The construct (pUAST-HA-*ScPpX1*-AttB) was injected into embryos for its integration in the AttP40 docking site in the second chromosome, and we recovered transgenic FLYX lines. We refer to these lines as Cyto-FLYX. We then validated the expression and localisation of HA-*Sc*PpX1 (driven by *da-GAL4*) using anti-HA antibody staining and found *Sc*PpX1 localisation throughout the cytoplasm **(Fig 4C, E)**. To test the polyP levels in FLYX, we used a *tubulin*-GAL4 driver, which allows ubiquitous expression of *HA-Sc*PpX1. We observed significantly decreased polyP content in Cyto-FLYX larvae compared with the control, suggesting that HA-*Sc*PpX1 can deplete polyP in flies **(Fig 4D)**.

To expand the *Drosophila* polyP depletion toolkit library, we engineered HA-*ScPpX1* constructs to facilitate subcellular compartment-specific depletion of polyP. We created FLYX lines that can target *Sc*PpX1 to the nucleus (Nuc-FLYX), endoplasmic reticulum (ER-FLYX), and the mitochondria (Mito-FLYX) **(Fig 4C)**. We tested the localisation of this FLYX in larval muscles using anti-HA antibody staining. We found that Nuc-FLYX intensely localises in the nuclear region devoid of DAPI (DNA) signal, suggesting probable nucleolar localisation; ER-FLYX co-localized with Calnexin, an ER protein; and Mito-FLYX co-localized with ComplexV subunit A, a mitochondrial protein **(Fig 4E, See Material and Methods for sequence)**. This FLYX library provides a handle for spatial polyP depletion in an organism to explore various physiological functions.

PolyP is crucial for hemolymph clotting.

Since hemocytes contribute to hemolymph clotting and *ex vivo* studies in humans have shown exogenous addition of polyP into blood plasma accelerates blood clotting, we reasoned that polyP may accelerate hemolymph clotting in flies (11,54–56). To assess and quantify hemolymph clotting characteristics, we established a 'hemolymph drop assay' **(Supplementary Fig 5A-E, see Material and Methods)**. The clotting hemolymph drop in this assay displays characteristic inward fibre-like structures perpendicular to the edge of the drop. These fibres are significantly reduced in length and number in the *hemolectin* (*hml*), a mutant known to exhibit hemolymph clotting defects **(Supplementary Fig 4A-E)** (57). Therefore, we used fibre number and characteristics to assess hemolymph clotting phenotypes. To test the effect of polyP on hemolymph clotting, we compared the clot characteristics of hemolymph mixed with water (blank), Pi (1.6 nmol Pi, negative control) or polyP of different average chain lengths (1.6 nmol polyP in Pi terms, equivalent to the total polyP content from two larvae). Upon exogenous addition of polyP, we found increased clot fibre numbers along the edge of the hemolymph drop **(Supplementary Fig 4F-J)**. Similar results were also observed when we reduced the concentration by half (125µM polyP (Pi terms) as has been used in human clotting studies) **(Supplementary Fig 5F-I)** (11,14). We found that the increase in the clot number density is dependent on the polyP chain length; $polyP_{14}$ did not increase the fibre numbers and length, while $PolyP_{65}$ and $PolyP_{130}$ led to a subtle and significant increase compared to blank and negative control samples **(Supplementary Fig 4K-V)**.

The observations that polyP can promote hemolymph clotting *ex vivo* and polyP is localised to large granular structures in hemocytes prompted us to test whether polyP is crucial for

hemolymph clotting *in vivo*. Thus, we tested the effect of polyP depletion by ubiquitous expression of *Sc*PpX1 on hemolymph clotting. We observed significantly lesser clot fibre numbers, branching points and clot fibre length in the Cyto-FLYX larvae (*tubulin*>Cyto-FLYX) than the control **(Fig 5A-D)**. These observations suggest that polyP is crucial for efficient hemolymph clotting.

We then sought to identify the cell type that contributes polyP for hemolymph clotting. Therefore, we decided to deplete polyP in a cell-specific manner using the FLYX system under three different drivers. We expressed Cyto-FLYX in fat bodies and all hemocytes using *cg*-GAL4 (*cg*>Cyto-FLYX) and observed reduced fibre length, clot fibre numbers and branching **(Fig 5E-H)**. We then used *hml*-GAL4 (*hml*>Cyto-FLYX), which mainly expresses in the plasmatocytes, and observed significantly reduced clot fibre number and branching densities. The clot fibre length, however, was comparable to the control **(Fig 5I-L)**. We did not observe any significant change in clot fibre numbers and branching when we expressed Cyto-FLYX only in crystal cells using *lz*-GAL4 (*lz*>Cyto-FLYX). The lengths of the clot fibres were also comparable to the control **(Fig 5M-P)**. These data suggest that polyP in hemocytes is necessary for efficient hemolymph clotting. Next, we tested the effect of exogenous addition of polyP in the clotting of hemolymph from *tubulin*>Cyto-FLYX flies. We divided hemolymph from *tubulin*>Cyto-FLYX flies into two parts and incubated one half with Pi (negative control) while the other half was incubated with $polyP_{65}$. On $polyP_{65}$ addition, we observed no significant rescue of the relative clot fibre numbers in *tubulin*>Cyto-FLYX compared to the control **(Fig 5Q-S)**. This suggests that intracellular polyP in the hemocytes might have a physiological role in the clot protein secretion. Taken together, the similarities in *ex vivo* clotting

studies in flies and humans and the *in vivo* studies in flies suggest that the cellular and molecular function of polyP in hemolymph/blood clotting are conserved between insects and mammals.

PolyP affects developmental timing

Since we observed differential regulation of polyP during development and in various tissues, we sought to systematically explore phenotypic expression upon ubiquitous depletion of polyP (*tubulin*>Cyto-FLYX). We found no significant differences in the weight or size of Cyto-FLYX vs. control larvae, pupae, or adults **(Supplementary Fig 6A-D).** Since the pUAST vector is not efficient in driving expression in the germ line cells, we cloned Cyto-FLYX in the pUASP vector and generated a new transgenic line to deplete polyP in the germ line cells. However, we found no significant change in the fecundity upon germ line expression of Cyto-FLYX using *Nos*-GAL4 driver **(Supplementary Fig 6E-F)**. Further, since we had observed polyP levels increase just before pupariation and decrease during pupal stages, we sought to test the impact of polyP depletion on the metamorphosis timing. We tested the total time taken from prepupae stages to the eclosion of adults when Cyto-FLYX is expressed ubiquitously (*tubulin*>Cyto-FLYX, **Fig 6A-B)**. Typically metamorphosis takes ~five days, we found *tubulin*>Cyto-FLYX required ~14 hours less for the eclosion of 50% pupae as compared to control (119.2 ± 3.863 hours for *tubulin*-Cyto-FLYX and 134.5 ± 4.877 hours for control). This data uncovers yet another impact of polyP on metazonal biology.

PolyP depletion affects a wide range of biological processes

Nutrient conditions and signalling pathways, such as Ecdysone, insulin and TOR are known to impact metamorphosis timing in flies. Third instar larvae undergoes multiple pulses of ecdysone signalling mediated through, among others, *ecd* (promotes metamorphosis), *Eip74EF* (ecdysteroid target gene of metamorphosis) (58). In synergy, the insulin signalling pathway promotes ecdysone signalling, and shows characteristic changes in expression of genes such as, insulin receptors (*inR*), insulin like peptides (*dilps*), *chico* (encoder of inR substrates), and *dfoxo* (insulin sensor gene) (59). Insulin signalling pathways via dFoxo also controls TOR signalling pathway effector genes such as, *4ebp* (60). We tested if the accelerated eclosion caused by polyP depletion is a result of transcriptomic changes in any of these aforementioned genes. We however, did not find a significant difference in the level of expression of genes- *ecd*, *ImpL2*, *Eip74EF*, *inR*, *chico*, *dfoxo*, *dilp2*, *tor*, *s6k*, and *4ebp* between *tubulin*>Cyto-FLYX and control third instar larvae suggesting that polyP may not directly impact Ecdysone, insulin and TOR pathways **(Supplementary Fig 7A)**.

To understand the cellular response to polyP depletion, we performed RNA sequencing of non-feeding time-matched third instar control and *tubulin-GAL4*>Cyto-FLYX larvae. Our data covered a total of 11747 genes, and the Principal Component Analysis (PCA) segregated the two genotypes in the major axis suggesting ubiquitous depletion of polyP changes the transcriptional landscape **(Supplementary Fig 7B)**. Using Gene Set Enrichment Analysis, with Gene Ontology annotations, we found a total of 262 sets of biological processes. We found translation and ribosome biogenesis pathways among the top ten upregulated biological processes, in the Cyto-FLYX third instar larvae. This is interesting as polyP has been proposed

to bind and modulate translation factors in other systems (61,62). Possible increase in translation could be a reason for accelerated developmental progression.

Among the gene sets downregulated in Cyto-FLYX third instar larvae, we found cell-cell adhesion and synaptic transmissions among the top ten hits. With the Cellular Component functional analyses, we also found downregulation of genes linked to neuronal projections and synapses in Cyto-FLYX larvae compared to control. Interestingly, synapses and dendritic connections are known to be pruned during larval to pupal transition as flies undergo neural circuit remodelling (63) **(Supplementary Fig 8A-D)**. In corroboration with the qPCR data, we did not find enrichment of genes linked to canonical ecdysone, TOR, and insulin pathways. Further, we also found enrichment of negative regulators of immune response in Cyto-FLYX larvae as compared to control. Humoral immune response in *Drosophila* is under ecdysone signalling influence, and it leads to downregulation of classical Toll and IMD pathways during larval to pupal transition. Thus, these Cyto-FLYX larvae might be susceptible to infections (64) **(See Supplementary table for RNA sequencing analysis)**. Although the transcriptomic analysis from whole larvae undermines tissue specific transcriptional changes, the wide range of impact of polyP depletion on whole larvae indicates a diverse role of polyP in organismal physiology.

Discussion:

Here we reported methods for quantification, visualisation, and genetic manipulation of polyP in flies. To quantify polyP levels, we streamlined a colorimetric-based protocol, and for detection of polyP in tissues, we used a GST-PPBD-based probe that specifically binds to polyP.

We investigated polyP levels in various developmental stages and tissue types and found that polyP levels are spatially, temporally, and developmentally regulated. Further, we created the FLYX system that allowed us to deplete polyP in sub-cellular and tissue-specific manner. Using FLYX we observed changes in the eclosion time of flies, suggesting the importance of the temporal polyP level regulation. We also reported that the polyP in plasmatocytes is crucial for hemolymph clotting, a process analogous to human blood clotting. With the evidence of the probable evolutionarily conserved function of polyP in flies and humans, the FLYX toolkit in flies provides a handle to explore novel functions of polyP. A possible limitation of this system is the lack of an inactive *Sc*PpX1 that can deplete polyP and thus can be used as a negative control to rule out any possible effects of overexpressing the exogenous protein.

Due to the inherent differences in polyP concentrations and chain lengths in different organisms, modifications in the polyP extraction and detection methods were required. To quantify polyP in flies we adopted the citrate-saturated phenol-chloroform-based method, which allows the purification of all chain lengths; however, with the caveat of copurification of RNA (34,35). Since RNA can interfere with polyP quantification, we incorporated an additional RNase treatment step into our extraction protocol. PolyP is often detected using DAPI, which, when bound to polyP and excited at 405 nm, emits fluorescence with a peak at 550 nm (65–68). This spectral property of DAPI-polyP has been exploited for polyP detection despite the interference from DAPI-RNA, which has a fluorescence emission maximum at 525 nm when excited at 405 nm. This interference may result in a false assessment of polyP levels, especially when polyP levels are very low and RNAse treatment may not be efficient in digesting the complete RNA (40). Thus, for the biochemical detection, we used an enzyme-based method that involves

enzymatic degradation of polyP, resulting in the release of Pi, which is then measured using Malachite Green (38,39). Further, to locate polyP in fly tissues, we utilised epitope-tagged PPBD, which specifically binds to polyP with a very high affinity (40,41). Using these tools, we assayed the polyP levels and their localization profiles across different fly developmental stages and in various tissue types, revealing spatiotemporal regulation of polyP in flies and providing a comprehensive estimation and distribution of polyP in a metazoan organism **(Fig 1-3, Supplementary Fig 1-3)**.

Comparative polyP levels across different developmental stages and tissue types in metazoans have yet to be assessed, and it is tempting to predict that differential regulation of polyP levels might be conserved during the development of all multicellular organisms due to complex and differential metabolic regulation. Intriguingly, though polyP level does not change significantly during the *Drosophila* embryonic development, we observed a significant increase in polyP level in the late larval stage, just before the pupariation, followed by a gradual decrease during metamorphosis (**Fig 1C-D**). We suspect that phosphates are synthesised and stored as a reservoir in the form of polyP during the late larval stage, which is then used during metamorphosis. An assessment of polyP levels during the development of *Dictyostelium discoideum*, a model that has been used to study the origin of multicellularity, revealed a 100-fold increase in polyP levels during the transition from a single cellular vegetative state to a multicellular fruiting body. This increase in polyP is necessary for metabolic regulation during the development of *Dictyostelium,* linking the necessity of polyP to the origin of multicellularity (69). Surprisingly, polyP-depleted flies (Cyto-FLYX) eclose faster **(Fig 6A-B)**, uncovering a yet unknown function of polyP during metamorphosis. Intriguingly, this faster eclosion did not

affect the size and weight of larvae and adults **(Supplementary Fig 6A-D)**. Although it is unclear why polyP depletion leads to shorter metamorphosis time, these observations could prompt several lines of phenotypic investigations to explore polyP functions.

Through our investigations, using PPBD probe, we found differential localisation of polyP in various subcellular compartments in a tissue specific manner. In most tissues, we found polyP localisation in the form of cytosolic puncta. While we do not know the identity of these structures, similar localization has been observed in platelet (dense granules) and mast cells (serotonin containing granules) (41,70) Strikingly, we observed intense PPBD staining in the nucleolus of salivary glands, muscle, crop, and wing disc cells. We also found nuclear targeted HA-*Sc*PpX1(Nuc-FLYX) localises in the nucleoli of the nucleus of muscle cells. These data indicate a nucleolar function of polyP in some cell types. The nucleolar polyP has also been previously reported in myeloma cells and cisplatin-treated HeLa cells (46,71). Nucleolar polyP has also been observed upon forced delivery of polyP into mammalian cells or by overexpression of polyP kinase in plant and mammalian cells (44,45,72). Since polyP can induce LLPS by its interactions with the nucleic acid and positively charged proteins, polyP may be involved in the organisation of the nucleolus, which is an LLPS organelle (45,73).

Overall, the polyP localization profile using GST-PPBD staining, which uncovered spatial and temporal regulation of polyP across various *Drosophila* tissues, would accelerate the discovery of various tissue-specific functions of polyP, particularly with the use of sophisticated fly genetic tools *in vivo* **(Fig 2-3, Supplementary Fig 3)**. That the fly gut microbiota can also potentially contribute to the polyP content in fly tissues is one important consideration. In this

article we allude to several observations that argue polyP is synthesized by fly tissues: (i) polyP levels remain very low during feeding stages but build up in wandering third instar larvae after feeding ceases **(Fig 1D)**; (ii) PPBD staining is absent from the gut except the crop **(Fig. S3O–P)**; and (iii) Recent work on *C.elegans* have reported polyP presence in the worm intestines, whereas in flies, polyP is present only in the crop with the rest of the gut containing undetectable amounts. Moreover, in *C. elegans*, intestinal polyP was unaffected when worms were fed polyP-deficient bacteria (43).

Recently, decreased polyP levels were found in the plasma of patients suffering from Type 1 Von Willebrand Disease (VWD) (12). Moreover, mice lacking the inositol pyrophosphate synthesising enzyme IP6K1 are reported to have reduced polyP levels and show blood clotting defects (13). Despite blood clotting being the best-known function of polyP in metazoans, studies on polyP-mediated blood clotting in mammals have been done by the *ex vivo* addition of polyP due to the limitation of direct genetic manipulations of polyP synthesis in platelets. Using FLYX- a transgenic fly system of polyP depletion, we show that polyP in plasmatocytes is crucial for hemolymph clotting **(Fig 5A-S)**. Studies in humans revealed that polyP localises inside granules in platelets, which, over the past two decades, have been shown to aid in mammalian blood clotting (70). Given our observation of the peripheral arrangement of polyP granules, we propose that polyP is either required for secretion, modification of clotting factors in plasmatocytes or contributes to the localised increase in polyP levels at the clotting site **(Fig 5Q-S)**. Our data also indicates the polyP in fat bodies also contributes to hemolymph clotting - notably, the length of clot fibres becomes significantly shorter when polyP is depleted in all hemocytes as well as fat bodies together but not when depleted only in plasmatocytes **(Fig 5H, L)**. As fat bodies are known to secrete hemolymph clotting factors, including proteins like

Fondue, which gets incorporated in the clots, polyP may modify or promote the secretion or activation of Fondue or any other factor crucial for fibre lengthening (74,75). Given conserved mechanisms of hemolymph and blood clotting, modelling polyP studies in flies can help understand the regulation, release and function of polyP during hemolymph and blood clotting.

The change in the whole larval transcriptome of Cyto-FLYX reiterates the myriad possibilities of polyP functions in metazoans. We performed GSEA due to the intra-sample variation (PC2 = 19.10%, **Supplementary Fig 7B**) as well as our aim to identify major differences in cellular responses/pathways between Cyto-FLYX and Control (76). The third instar larval population usually undergoes bursts of transcription related to its development and metamorphosis. Through GSEA, we found gene sets enriched for translation and ribosome biogenesis **(Supplementary Fig 8A-D)**. Indeed, the proteomic analysis of a Δ*ppk* mutant *E.coli*, which results in absence of polyP, also shows a similar response (77). The reason for the increase in such biological processes in the absence of polyP (either due to no polyP synthesis or polyP depletion) remains to be investigated. Earlier polyP binding assays have shown that polyP can bind to proteins associated with translation. By linking polyP depletion to both increased translational gene expression and accelerated developmental progression, we are tempted to hypothesize a mechanistic axis in which polyP restrains protein synthesis to coordinate the timing of metamorphosis. Overall, by cytoplasmic depletion of polyP with the FLYX toolkit, we demonstrated the conservation of polyP function in hemolymph/blood clotting and the importance of polyP regulation during metamorphosis.

Through transcriptomics, followed by Gene Set Enrichment Analysis, we found the impact of cytoplasmic polyP in several biological processes including translation and ribosome biogenesis

processes during late larval stage, reiterating the myriad possibilities of polyP functions in metazoans. An unbiased phenotypic analysis following polyP depletion in various tissues and subcellular compartments using FLYX lines developed in this work would facilitate the discovery of many unknown functions of polyP. Further, the use of *Drosophila* genetic epistatic studies, by combining spatial and temporal regulation of polyP with structure and function analysis would be useful in assigning biological meaning to several metazoan polyphosphorylated proteins that have been identified in recent studies (19–21). Finally, given the recent implications of polyP in human diseases, the fly model would be a valuable and unique *in vivo* system to uncover the pathogenic mechanisms of polyP-linked diseases.

In summary, this study establishes *Drosophila* as a much-needed metazoan model for polyphosphate biology, revealing conserved roles in clotting and development. The tools and findings presented here will pave the ways for new investigations to uncover functions of this ancient polymer in animal biology and its implications in human diseases.

Materials and methods:

Polyphosphate quantification using malachite green Assay:

Malachite green (MG) detects monophosphates released from polyP pools due to the addition of purified yeast exopolyphosphatase (*Sc*PpX1). Samples with extracted polyP were divided into two parts; one part was treated with 5ug/ml *Sc*PpX1 for 18 hours at 37°C while the other half acted as the untreated control. MG reagent was prepared by mixing MG (0.045% in water) and Ammonium molybdate (4.2% in 4N HCl) in 3:1(vol/vol) ratio and filtered through a Whatman grade 1 paper. K_2HPO_4 (0.1 – 20 nmoles) was used as a phosphate standard. Samples or standards (50 µl) were loaded into 96 healthy plates, and 200 µl of MG reagent was added per sample, followed by incubation in the dark for 15 minutes at room temperature. Absorbance was measured at 650 nm using the Omega PolarStar Plate Reader. PolyP content of the samples (in Pi terms) was determined by interpolation from a linear regression analysis of the K_2HPO_4 standard.

GST-PPBD staining:

Tissues were dissected in 1X TBS (Tris Buffered Saline - 50mM Tris-HCl pH 7.6, 150mM NaCl), and fixed in 4% paraformaldehyde for 20 minutes. They were then subjected to three 1X TBST (TBS with 0.2% Triton X-100) washes for ten minutes each. 5% NGS (nascent goat serum) was added to the tissues as a blocking agent, and incubated for one hour at room temperature. The tissues were next incubated with 25ng/µl GST or GST-PPBD (purification process mentioned in GST and GST-PPBD Protein Purification section of methods) for one hour at room temperature followed by three 1X TBST washes for ten minutes each. The tissues were then incubated in mouse anti-GST antibodies overnight at 4℃. The next day, the tissues

were washed thrice with 1X TBST and incubated with goat anti-mouse antibody conjugated with Alexa555 dye at room temperature for two hours. Following incubation, the tissues were washed thrice with 1X TBST and incubated with 100µM DAPI to stain nuclei for 15 minutes at room temperature. DAPI staining was followed by a final step of three washes with 1X TBST before mounting the dissected tissues on slides for imaging. Images were acquired with a Leica STELLARIS 5 confocal microscope.

For colocalisation with nucleolus, Rabbit anti-Fibrillarin antibody was incubated with the primary Mouse anti-GST antibodies overnight at 4℃. The next day, the tissues were washed thrice with 1X TBST and incubated with goat anti-mouse antibody conjugated with Alexa555, and goat anti-rabbit antibody conjugated with Alexa488 dye at room temperature for two hours. This was followed by a final step of three washes with 1X TBST before mounting the dissected tissues on slides for imaging. Images were acquired with a Leica STELLARIS 5 confocal microscope. Figures of Supplementary 3A-B were imaged with Nikon microscope CSU-W1.

Creation of FLYX - transgenic *Sc*PpX1 flies:

The *ScPpX1* gene sequence from pTrc-HisB-*ScPpX1* was codon optimised for *Drosophila melanogaster* in open access platform Benchling. The codon-optimised *ScPpX1* sequence **(See Supplementary material)** was tagged with HA epitope (TATCCGTATGATGTTCCGGATTATGCA) in the N-terminal region, and flanked by restriction sites EcoRI and XbaI. The entire fragment was synthesised by GeneScript. The HA-*ScPpX1* was cloned out from the carrier vector using restriction sites EcoR1 and Xba1 into fly expression vector pUAST-attB. The plasmid was then injected into embryos for site-directed

transgenesis in the second chromosome using the *y; AttP40* flies. Two independent lines (Cyto-FLYX) were generated, and one was used in the experiments of this study.

For targeted *Sc*PpX1 expression, the codon-optimised *ScPpX1* sequence **(See Supplementary material)** was tagged with HA epitope (TATCCGTATGATGTTCCGGATTATGCA) in the N-terminal region following the 3XNLS (nuclear localisation signal) for Nuc-FLYX, Cox8A signal sequence for Mito-FLYX, and the KDEL sequence for ER-FLYX. The gene inserts **(See Supplementary material)** were all flanked by restriction sites EcoRI and XbaI. The entire fragment was synthesised by GeneScript. The HA-*ScPpX1* was cloned out from the carrier vector using restriction sites EcoR1 and Xba1 into fly expression vector pUAST-attB. The plasmid was then injected into embryos for site-directed transgenesis in the second chromosome using the *y; AttP40* flies. Two independent lines were generated, and one was used in the experiments of this study.

For expression in the gonads, the Cyto-FLYX construct was subcloned into pUASp vector, and three independent lines based on p-element insertions in the second chromosome were identified and retrieved.

Immunohistochemistry :

Larval filae were prepared for staining muscle cells for HA expression in GAL4 driven FLYX lines in 1X TBS (Tris Buffered Saline - 50mM Tris-HCl pH 7.6, 150mM NaCl), and fixed in 4% paraformaldehyde for 20 minutes. They were then subjected to three 1X TBST (TBS with 0.2% Triton X-100) washes for ten minutes each. 5% NGS (nascent goat serum) was added to the tissues as a blocking agent, and incubated for one hour at room temperature. For Cyto-FLYX and Nuc-FLYX, to stain HA, we used mouse anti-HA primary antibody whereas,

for ER-FLYX and Mito-FLYX, to stain HA, we used rabbit anti-HA primary antibody, mouse anti-KDEL primary antibody (ER-F:YX) and mouse anti-ATP5A (Mito-FLYX) primary antibody. The tissues were incubated overnight at 4℃. The next day, the tissues were washed thrice with 1X TBST and incubated with goat anti-mouse antibody conjugated with Alexa555, and goat anti-rabbit antibody conjugated with Alexa488 dye at room temperature for two hours. The tissues were washed thrice with 1X TBST buffer. For Cyto-FLYX and Nuc-FLYX, after the secondary antibody incubation and washing, tissues were incubated with 100µM DAPI to stain nuclei for 15 minutes at room temperature. This was followed by a final step of three washes with 1X TBST before mounting the dissected tissues on slides for imaging. Images were acquired with a Leica STELLARIS 5 confocal microscope.

Hemocyte adherence and immunostaining

For adherence, the hemolymph was collected from 10 larvae in 15µl TBS and allowed to adhere on a glass slide at room temperature for 30 minutes - the method adopted by Hankde et.al. 2013 (78). The supernatant was taken out carefully, and the adhered cells were fixed using 4% PFA for 20 minutes. This was followed by immunostaining with GST-PPBD using the GST-PPBD staining procedure mentioned above.

For treatment of hemocytes with *Sc*PpX1 and heat inactivated *Sc*PpX1, hemocytes were subjected to three 1X TBST (TBS with 0.2% Triton X-100) washes for ten minutes each, and then incubated with 5ug/ml of *Sc*PpX1 in 1X TBS or heat inactivated *Sc*PpX1 in 1X TBS (incubated protein at 65℃ for 30minutes) at 37℃ for 2 hours. The control untreated hemocytes were also given the same incubation at 37℃ for 2 hours. This was followed by three washes and immunostaining with GST-PPBD using the GST-PPBD staining procedure mentioned above.

Assessment of clot fibre characteristics

For assessment of the clot fibre parameters - number, branching, and length- 20 larvae were collected, washed in 1X TBS and dried on tissue paper. The dorsal side mouth hook region was gently torn to let only the hemolymph ooze out. For **Supplementary Fig 5F-J,** and **Supplementary Fig 6**, the hemolymph was collected and divided into two sets of 2µl drops. 2µl hemolymph was mixed with either 1µl water or 1µl Pi (0.8 nmole) as control, and 1µl PolyP ($PolyP_{14}$, $PolyP_{65}$, $PolyP_{130,}$ each containing 0.8 nmole in Pi terms) as test samples. For **Supplementary Fig 5B-C, and Fig 5**, the hemolymph was collected, and 2µl was mixed with 1µl of water in each of the cases tested. The slide was incubated at room temperature (24°C) for 25-30 minutes to allow evaporation. Post-incubation, clot fibres were imaged using an Olympus BX53 upright microscope with a 10X objective lens fitted with a Retiga-R6 camera. Post imaging, the number of fibres, fibre branch points, fibre length, and circumference of the clot were measured manually using ImageJ analysis software. The number of fibres, branch points, and length of fibres were then normalised to the circumference of the respective clot. The mean of the normalised data sets of the control was analysed. Every data set is represented as relative to the mean of the normalised data of the control.

Eclosion kinetic study:

To study pupal eclosion kinetics, flies were allowed to lay eggs for 12 hours, after which 150 first instar larvae were collected in a span of 30 minutes to have a synchronous culture and grown at 25ºC. White prepupa were collected after 6 days and staged again. The time of collection of white prepupa was set to T=0. The time of eclosion of flies was noted. A total of

213 control flies, and 268 FLYX were scored for eclosion in three independent sets. Only plates from where at least 25 flies eclosed in a day were considered for the study.

RNA Transcriptome analysis

Sets of five larvae were subjected to RNA isolation using TRIzol (Ambion life tech—15596018) method. The RNA library was prepared using NEBNext® Ultra™ II Directional RNA Library Prep with Sample Purification Beads. Downstream analyses were done in the condo (23.7.4) and R (4.3.2) environments. Briefly, raw reads were pair-end pseudo-aligned to the annotated *Drosophila melanogaster* genome (BDGP6.32) dataset using Kallisto (0.48.0) (79) and imported to the R environment. Uniquely mapped reads were further filtered and normalised using the Trimmed mean of M-values (TMM) (80) method of EdgeR/limma (4.0.3) Bioconductor library (81).

Then, Gene Set Enrichment Analysis (GSEA) (82) was performed using the clusterProfiler (4.10.1) package (83). In essence, gseGO functions were used to identify the GSEA of Gene Ontology for Biological Processes (BP), Molecular Functions (MF) and Cellular Components (CC).

Code Availability

The code is available in the supplementary text.

Graph and statistical analysis:

All the graphs and statistical analysis were done using GraphPad Prism software. The statistical tests used are mentioned in the respective figure legends.

Acknowledgements

We thank Adolfo Saiardi for his kind gift of plasmid pTrc-HisB-*ScPpX1*. We also thank T. Shiba for generously sharing polyP of different chain lengths -polyP ($PolyP_{14}$, $PolyP_{65}$, $PolyP_{130}$). We thank Shubham Kumar Agrawal for help with the purification of *Sc*PpX1 and Manisha Mallick for assisting PPX and PPBD binding experiments. We acknowledge Debaditya De, Aditya Rane, and Manasa Chanduri for the construction of the *ScPpX1* and GST-PPBD expression plasmids. We thank Rakesh Mahato for assisting in the MST experiments and Dr. Pankaj Suman for sharing the MST set up at the National Institute of Animal Biotechnology, India. We thank Lolitika Mandal for sharing *HmlGAL4>UAS GFP* fly lines with us. We thank Aprotim Mazumder for sharing anti-Fibrillarin antibodies. We thank Vipin Agarwal for sharing the SEC setup for protein purification. We thank Dr. Deepti Trivedi and NCBS fly facility for injections and Dr. Awadhesh Pandit and his team at NCBS for RNA library preparation and RNA sequencing. We thank Kalyaneswar Mandal, Sonal Nagarkar Jaiswal and members of the Laboratory of Cell Signalling CDFD and MJ lab TIFRH for discussions and valuable feedback. We thank Anand T Vaidya, Vinay Bulusu and Oguz Kanca for the critical reading, comments and valuable suggestions on the manuscript.

Funding

This work is funded by DBT-DFG grant IC12025(11)/2/2020-ICD-DBT to MJ and RB. MJ is supported by the Department of Atomic Energy (Project Identification No. RTI4007), Department of Science and Technology, SERB (CRG/2020/003275), Department of Biotechnology (BT/PR32873/BRB/10/1850/2020), Government of India. MJ was a Ramalingaswami fellow of the Department of Biotechnology, Government of India, under

project number BT/RLF/Re-entry/06/2016. R.B. acknowledges support from the Department of Biotechnology, Ministry of Science and Technology, Govt. of India. (BT/PR29960/BRB/10/1762/2019); Science and Engineering Research Board, Department of Science and Technology, Govt. of India (CRG/2019/002597); and CDFD core funds. HJ acknowledges funding for this project by the Deutsche Forschungsgemeinschaft (DFG, German Research Foundation, project number 445698446) in collaboration with the Indian Department of Biotechnology (DBT). Moreover, this work was supported by the Deutsche Forschungsgemeinschaft (DFG) under Germany's Excellence Strategy (CIBSS-EXC-2189-Project ID 390939984, to HJJ). SS is an Infosys fellow (Leading Edge TG/(R-11)/09/). A Shyama Prasad Mukherjee Fellowship from the Council of Scientific and Industrial Research, Government of India, supports JSL.

Author contributions

SS, RB and MJ have conceptualised the study. SS: Designed the methods, validated, and performed most experiments and analysed the data. HS: GST and GST-PPBD labelling, hemolymph clotting experiments along with SS. SM: Synthesis of PolyP-100-2X-FITC. JSL: Analysis of polyphosphate by gel electrophoresis, and assistance in initial polyP characterisation in flies. SKYH: RNA transcriptome analysis and fecundity experiment. DB: RNA extraction and qRT-PCR. SRK: Size Exclusion Chromatography for *Sc*PpX1 purification. SS and MJ wrote the original draft. Everyone has reviewed and edited the manuscript. MJ and RB supervised the study. MJ and RB were responsible for the project administration and funding acquisition.

References:

1. Wiame JM. The metachromatic reaction of hexametaphosphate. J Am Chem Soc. 1947 Dec;69(12):3146.
2. Achbergerová L, Nahálka J. Polyphosphate--an ancient energy source and active metabolic regulator. Microb Cell Fact. 2011 Aug 4;10:63.
3. Kornberg A, Rao NN, Ault-Riché D. Inorganic polyphosphate: a molecule of many functions. Annu Rev Biochem. 1999;68:89–125.
4. Kornberg A. Inorganic polyphosphate: toward making a forgotten polymer unforgettable. J Bacteriol. 1995 Feb;177(3):491–6.
5. Cremers CM, Knoefler D, Gates S, Martin N, Dahl J-U, Lempart J, et al. Polyphosphate: A conserved modifier of amyloidogenic processes. Mol Cell. 2016 Sep 1;63(5):768–80.
6. Wang X, Shi C, Mo J, Xu Y, Wei W, Zhao J. An inorganic biopolymer polyphosphate controls positively charged protein phase transitions. Angew Chem Int Ed. 2020 Feb 10;59(7):2679–83.
7. Beaufay F, Amemiya HM, Guan J, Basalla J, Meinen BA, Chen Z, et al. Polyphosphate drives bacterial heterochromatin formation. Sci Adv. 2021 Dec 24;7(52):eabk0233.
8. Dunn T, Gable K, Beeler T. Regulation of cellular Ca2+ by yeast vacuoles. J Biol Chem. 1994 Mar 11;269(10):7273–8.
9. Archibald FS, Fridovich I. Investigations of the state of the manganese in Lactobacillus plantarum. Arch Biochem Biophys. 1982 May;215(2):589–96.
10. Pick U, Weiss M. Polyphosphate Hydrolysis within Acidic Vacuoles in Response to Amine-Induced Alkaline Stress in the Halotolerant Alga Dunaliella salina. Plant Physiol. 1991 Nov;97(3):1234–40.
11. Smith SA, Mutch NJ, Baskar D, Rohloff P, Docampo R, Morrissey JH. Polyphosphate modulates blood coagulation and fibrinolysis. Proc Natl Acad Sci USA. 2006 Jan 24;103(4):903–8.
12. Montilla M, Hernández-Ruiz L, García-Cozar FJ, Alvarez-Laderas I, Rodríguez-Martorell J, Ruiz FA. Polyphosphate binds to human von Willebrand factor in vivo and modulates its interaction with glycoprotein Ib. J Thromb Haemost. 2012 Nov;10(11):2315–23.
13. Ghosh S, Shukla D, Suman K, Lakshmi BJ, Manorama R, Kumar S, et al. Inositol hexakisphosphate kinase 1 maintains hemostasis in mice by regulating platelet polyphosphate levels. Blood. 2013 Aug 22;122(8):1478–86.
14. Smith SA, Choi SH, Davis-Harrison R, Huyck J, Boettcher J, Rienstra CM, et al. Polyphosphate exerts differential effects on blood clotting, depending on polymer size. Blood. 2010 Nov 18;116(20):4353–9.

15. Seidlmayer LK, Gomez-Garcia MR, Blatter LA, Pavlov E, Dedkova EN. Inorganic polyphosphate is a potent activator of the mitochondrial permeability transition pore in cardiac myocytes. J Gen Physiol. 2012 May;139(5):321–31.

16. Holmström KM, Marina N, Baev AY, Wood NW, Gourine AV, Abramov AY. Signalling properties of inorganic polyphosphate in the mammalian brain. Nat Commun. 2013;4:1362.

17. Wang Y, Li M, Li P, Teng H, Fan D, Du W, et al. Progress and applications of polyphosphate in bone and cartilage regeneration. Biomed Res Int. 2019 Jun 27;2019:5141204.

18. Omelon S, Georgiou J, Henneman ZJ, Wise LM, Sukhu B, Hunt T, et al. Control of vertebrate skeletal mineralization by polyphosphates. PLoS ONE. 2009 May 20;4(5):e5634.

19. Azevedo C, Singh J, Steck N, Hofer A, Ruiz FA, Singh T, et al. Screening a Protein Array with Synthetic Biotinylated Inorganic Polyphosphate To Define the Human PolyP-ome. ACS Chem Biol. 2018 Aug 17;13(8):1958–63.

20. Azevedo C, Livermore T, Saiardi A. Protein polyphosphorylation of lysine residues by inorganic polyphosphate. Mol Cell. 2015 Apr 2;58(1):71–82.

21. Neville N, Lehotsky K, Yang Z, Klupt KA, Denoncourt A, Downey M, et al. Modification of histidine repeat proteins by inorganic polyphosphate. Cell Rep. 2023 Sep 26;42(9):113082.

22. Arredondo C, Cefaliello C, Dyrda A, Jury N, Martinez P, Díaz I, et al. Excessive release of inorganic polyphosphate by ALS/FTD astrocytes causes non-cell-autonomous toxicity to motoneurons. Neuron. 2022 May 18;110(10):1656-1670.e12.

23. Fujiya M, Ueno N, Kashima S, Tanaka K, Sakatani A, Ando K, et al. Long-Chain Polyphosphate Is a Potential Agent for Inducing Mucosal Healing of the Colon in Ulcerative Colitis. Clin Pharmacol Ther. 2020 Feb;107(2):452–61.

24. Desfougères Y, Saiardi A, Azevedo C. Inorganic polyphosphate in mammals: where's Wally? Biochem Soc Trans. 2020 Feb 28;48(1):95–101.

25. Zhu Y, Huang W, Lee SSK, Xu W. Crystal structure of a polyphosphate kinase and its implications for polyphosphate synthesis. EMBO Rep. 2005 Jul;6(7):681–7.

26. Wei ZZ, Vatcher G, Tin AHY, Teng JL, Wang J, Cui QH, et al. Positively-charged semi-tunnel is a structural and surface characteristic of polyphosphate-binding proteins: an in-silico study. PLoS ONE. 2015 Apr 16;10(4):e0123713.

27. Rangarajan ES, Nadeau G, Li Y, Wagner J, Hung M-N, Schrag JD, et al. The structure of the exopolyphosphatase (PPX) from Escherichia coli O157:H7 suggests a binding mode for long polyphosphate chains. J Mol Biol. 2006 Jun 23;359(5):1249–60.

28. Bolesch DG, Keasling JD. Polyphosphate binding and chain length recognition of Escherichia coli exopolyphosphatase. J Biol Chem. 2000 Oct 27;275(43):33814–9.

29. Ugochukwu E, Lovering AL, Mather OC, Young TW, White SA. The crystal structure of the cytosolic exopolyphosphatase from Saccharomyces cerevisiae reveals the basis for substrate specificity. J Mol Biol. 2007 Aug 24;371(4):1007–21.

30. Alvarado J, Ghosh A, Janovitz T, Jauregui A, Hasson MS, Sanders DA. Origin of exopolyphosphatase processivity: Fusion of an ASKHA phosphotransferase and a cyclic nucleotide phosphodiesterase homolog. Structure. 2006 Aug;14(8):1263–72.

31. Baev AY, Angelova PR, Abramov AY. Inorganic polyphosphate is produced and hydrolyzed in F0F1-ATP synthase of mammalian mitochondria. Biochem J. 2020 Apr 30;477(8):1515–24.

32. Tammenkoski M, Koivula K, Cusanelli E, Zollo M, Steegborn C, Baykov AA, et al. Human metastasis regulator protein H-prune is a short-chain exopolyphosphatase. Biochemistry. 2008 Sep 9;47(36):9707–13.

33. Samper-Martín B, Sarrias A, Lázaro B, Pérez-Montero M, Rodríguez-Rodríguez R, Ribeiro MPC, et al. Polyphosphate degradation by Nudt3-Zn2+ mediates oxidative stress response. Cell Rep. 2021 Nov 16;37(7):110004.

34. Bru S, Jiménez J, Canadell D, Ariño J, Clotet J. Improvement of biochemical methods of polyP quantification. Microb Cell. 2016 Dec 29;4(1):6–15.

35. Christ JJ, Willbold S, Blank LM. Methods for the analysis of polyphosphate in the life sciences. Anal Chem. 2020 Mar 17;92(6):4167–76.

36. Christ JJ, Blank LM. Enzymatic quantification and length determination of polyphosphate down to a chain length of two. Anal Biochem. 2018 May 1;548:82–90.

37. Van Veldhoven PP, Mannaerts GP. Inorganic and organic phosphate measurements in the nanomolar range. Anal Biochem. 1987 Feb 15;161(1):45–8.

38. Petitou M, Tuy F, Rosenfeld C. A simplified procedure for organic phosphorus determination from phospholipids. Anal Biochem. 1978 Nov;91(1):350–3.

39. Hohenwallner W, Wimmer E. The Malachite green micromethod for the determination of inorganic phosphate. Clin Chim Acta. 1973 Apr 30;45(2):169–75.

40. Saito K, Ohtomo R, Kuga-Uetake Y, Aono T, Saito M. Direct labeling of polyphosphate at the ultrastructural level in Saccharomyces cerevisiae by using the affinity of the polyphosphate binding domain of Escherichia coli exopolyphosphatase. Appl Environ Microbiol. 2005 Oct;71(10):5692–701.

41. Moreno-Sanchez D, Hernandez-Ruiz L, Ruiz FA, Docampo R. Polyphosphate is a novel pro-inflammatory regulator of mast cells and is located in acidocalcisomes. J Biol Chem. 2012 Aug 17;287(34):28435–44.

42. Negreiros RS, Lander N, Huang G, Cordeiro CD, Smith SA, Morrissey JH, et al. Inorganic polyphosphate interacts with nucleolar and glycosomal proteins in trypanosomatids. Mol Microbiol. 2018 Dec;110(6):973–94.

43. Quarles E, Petreanu L, Narain A, Jain A, Rai A, Wang J, et al. Cryosectioning and immunofluorescence of C. elegans reveals endogenous polyphosphate in intestinal endo-lysosomal organelles. Cell Rep Methods. 2024 Oct 8;100879.

44. Fernandes-Cunha GM, McKinlay CJ, Vargas JR, Jessen HJ, Waymouth RM, Wender PA. Delivery of Inorganic Polyphosphate into Cells Using Amphipathic Oligocarbonate Transporters. ACS Cent Sci. 2018 Oct 24;4(10):1394–402.

45. Borghi F, Azevedo C, Johnson E, Burden JJ, Saiardi A. A mammalian model reveals inorganic polyphosphate channeling into the nucleolus and induction of a hyper-condensate state. Cell Rep Methods. 2024 Jul 15;4(7):100814.

46. Jimenez-Nuñez MD, Moreno-Sanchez D, Hernandez-Ruiz L, Benítez-Rondán A, Ramos-Amaya A, Rodríguez-Bayona B, et al. Myeloma cells contain high levels of inorganic polyphosphate which is associated with nucleolar transcription. Haematologica. 2012 Aug;97(8):1264–71.

47. Nakamura A, Kawano N, Motomura K, Kuroda A, Sekiguchi K, Miyado M, et al. Degradation of phosphate polymer polyP enhances lactic fermentation in mice. Genes Cells. 2018 Oct 1;23(10):904–14.

48. Motta LS, Ramos IB, Gomes FM, de Souza W, Champagne DE, Santiago MF, et al. Proton-pyrophosphatase and polyphosphate in acidocalcisome-like vesicles from oocytes and eggs of Periplaneta americana. Insect Biochem Mol Biol. 2009 Mar;39(3):198–206.

49. Gomes FM, Ramos IB, Motta LM, Miranda K, Santiago MF, de Souza W, et al. Polyphosphate polymers during early embryogenesis of Periplaneta americana. J Insect Physiol. 2008 Dec;54(12):1459–66.

50. Wang L, Fraley CD, Faridi J, Kornberg A, Roth RA. Inorganic polyphosphate stimulates mammalian TOR, a kinase involved in the proliferation of mammary cancer cells. Proc Natl Acad Sci USA. 2003 Sep 30;100(20):11249–54.

51. Duffy JB. GAL4 system in Drosophila: a fly geneticist's Swiss army knife. Genesis. 2002;34(1–2):1–15.

52. Brand AH, Perrimon N. Targeted gene expression as a means of altering cell fates and generating dominant phenotypes. Development. 1993 Jun;118(2):401–15.

53. Groth AC, Fish M, Nusse R, Calos MP. Construction of transgenic Drosophila by using the site-specific integrase from phage phiC31. Genetics. 2004 Apr;166(4):1775–82.

54. Morrissey JH, Smith SA. Polyphosphate as modulator of hemostasis, thrombosis, and inflammation. J Thromb Haemost. 2015 Jun;13 Suppl 1:S92-7.

55. Baker CJ, Smith SA, Morrissey JH. Polyphosphate in thrombosis, hemostasis, and inflammation. Res Pract Thromb Haemost. 2019 Jan;3(1):18–25.

56. Morrissey JH, Choi SH, Smith SA. Polyphosphate: an ancient molecule that links platelets, coagulation, and inflammation. Blood. 2012 Jun 21;119(25):5972–9.

57. Scherfer C, Karlsson C, Loseva O, Bidla G, Goto A, Havemann J, et al. Isolation and characterization of hemolymph clotting factors in Drosophila melanogaster by a pullout method. Curr Biol. 2004 Apr 6;14(7):625–9.

58. Baehrecke EH. Ecdysone signaling cascade and regulation of Drosophila metamorphosis. Arch Insect Biochem Physiol. 1996;33(3–4):231–44.

59. Shingleton AW, Das J, Vinicius L, Stern DL. The temporal requirements for insulin signaling during development in Drosophila. PLoS Biol. 2005 Sep;3(9):e289.

60. Koyama T, Mendes CC, Mirth CK. Mechanisms regulating nutrition-dependent developmental plasticity through organ-specific effects in insects. Front Physiol. 2013 Sep 26;4:263.

61. Bentley-DeSousa A, Holinier C, Moteshareie H, Tseng Y-C, Kajjo S, Nwosu C, et al. A screen for candidate targets of lysine polyphosphorylation uncovers a conserved network implicated in ribosome biogenesis. Cell Rep. 2018 Mar 27;22(13):3427–39.

62. Baijal K, Abramchuk I, Herrera CM, Mah T-F, Trent MS, Lavallée-Adam M, et al. Polyphosphate kinase regulates LPS structure and polymyxin resistance during starvation in E. coli. PLoS Biol. 2024 Mar 13;22(3):e3002558.

63. Yaniv SP, Schuldiner O. A fly's view of neuronal remodeling. Wiley Interdiscip Rev Dev Biol. 2016 Sep;5(5):618–35.

64. Verma P, Tapadia MG. Early gene Broad complex plays a key role in regulating the immune response triggered by ecdysone in the Malpighian tubules of Drosophila melanogaster. Mol Immunol. 2015 Aug;66(2):325–39.

65. Omelon S, Georgiou J, Habraken W. A cautionary (spectral) tail: red-shifted fluorescence by DAPI-DAPI interactions. Biochem Soc Trans. 2016 Feb;44(1):46–9.

66. Kulakova AN, Hobbs D, Smithen M, Pavlov E, Gilbert JA, Quinn JP, et al. Direct quantification of inorganic polyphosphate in microbial cells using 4'-6-diamidino-2-phenylindole (DAPI). Environ Sci Technol. 2011 Sep 15;45(18):7799–803.

67. Aschar-Sobbi R, Abramov AY, Diao C, Kargacin ME, Kargacin GJ, French RJ, et al. High sensitivity, quantitative measurements of polyphosphate using a new DAPI-based approach. J Fluoresc. 2008 Sep;18(5):859–66.

68. Tanious FA, Veal JM, Buczak H, Ratmeyer LS, Wilson WD. DAPI (4',6-diamidino-2-phenylindole) binds differently to DNA and RNA: minor-groove

binding at AT sites and intercalation at AU sites. Biochemistry. 1992 Mar 31;31(12):3103–12.

69. Livermore TM, Chubb JR, Saiardi A. Developmental accumulation of inorganic polyphosphate affects germination and energetic metabolism in Dictyostelium discoideum. Proc Natl Acad Sci USA. 2016 Jan 26;113(4):996–1001.

70. Ruiz FA, Lea CR, Oldfield E, Docampo R. Human platelet dense granules contain polyphosphate and are similar to acidocalcisomes of bacteria and unicellular eukaryotes. J Biol Chem. 2004 Oct 22;279(43):44250–7.

71. Xie L, Rajpurkar A, Quarles E, Taube N, Rai AS, Erba J, et al. Accumulation of Nucleolar Inorganic Polyphosphate Is a Cellular Response to Cisplatin-Induced Apoptosis. Front Oncol. 2019 Dec 12;9:1410.

72. Lorenzo-Orts L, Hohmann U, Zhu J, Hothorn M. Molecular characterization of CHAD domains as inorganic polyphosphate-binding modules. Life Sci Alliance. 2019 Jun;2(3).

73. Chawla R, Klupt S, Patsalo V, Williamson JR, Racki LR. The Histone H1-Like Protein AlgP Facilitates Even Spacing of Polyphosphate Granules in Pseudomonas aeruginosa. MBio. 2022 Jun 28;13(3):e0246321.

74. Lindgren M, Riazi R, Lesch C, Wilhelmsson C, Theopold U, Dushay MS. Fondue and transglutaminase in the Drosophila larval clot. J Insect Physiol. 2008 Mar;54(3):586–92.

75. Schmid MR, Dziedziech A, Arefin B, Kienzle T, Wang Z, Akhter M, et al. Insect hemolymph coagulation: Kinetics of classically and non-classically secreted clotting factors. Insect Biochem Mol Biol. 2019 Jun;109:63–71.

76. Chicco D, Agapito G. Nine quick tips for pathway enrichment analysis. PLoS Comput Biol. 2022 Aug 11;18(8):e1010348.

77. Baijal K, Abramchuk I, Herrera CM, Stephen Trent M, Lavallée-Adam M, Downey M. Proteomics analysis reveals a role for E. coli polyphosphate kinase in membrane structure and polymyxin resistance during starvation. BioRxiv. 2023 Jul 6;

78. Handke B, Poernbacher I, Goetze S, Ahrens CH, Omasits U, Marty F, et al. The hemolymph proteome of fed and starved Drosophila larvae. PLoS ONE. 2013 Jun 20;8(6):e67208.

79. Bray NL, Pimentel H, Melsted P, Pachter L. Near-optimal probabilistic RNA-seq quantification. Nat Biotechnol. 2016 May;34(5):525–7.

80. Robinson MD, Oshlack A. A scaling normalization method for differential expression analysis of RNA-seq data. Genome Biol. 2010 Mar 2;11(3):R25.

81. Robinson MD, McCarthy DJ, Smyth GK. edgeR: a Bioconductor package for differential expression analysis of digital gene expression data. Bioinformatics. 2010 Jan 1;26(1):139–40.

82. Subramanian A, Tamayo P, Mootha VK, Mukherjee S, Ebert BL, Gillette MA, et al. Gene set enrichment analysis: a knowledge-based approach for interpreting genome-wide expression profiles. Proc Natl Acad Sci USA. 2005 Oct 25;102(43):15545–50.

83. Wu T, Hu E, Xu S, Chen M, Guo P, Dai Z, et al. clusterProfiler 4.0: A universal enrichment tool for interpreting omics data. Innovation (Camb). 2021 Aug 28;2(3):100141.

84. Blanca Lázaro, Francisco J. Tadeo-Masa, Andrea Rodriguez, Lucia Ayuso, Joan M Martínez-Láinez, Eva Quandt, Maribel Bernard, Filipy Borghi, Adolfo Saiardi, Jonàs Juan-Mateu, Javier Jiménez, Josep Clotet, Samuel Bru, Nuclear Speckle Dynamics are Controlled by Polyphosphate Inhibition of CLK Proteins. bioRxiv 2025.01.15.633116, doi: https://doi.org/10.1101/2025.01.15.633116

Figure legends:

Fig 1: Polyphosphate extraction and quantification from flies. A) Linear polyphosphate. **B)** PolyP quantification from sets of 5, 10, 20 third instar larvae (in Pi terms), N=5 in each set. Statistics: Student's *t*-test $p > 0.001$, error bar - s.e.m. *Drosophila* strain used - *CantonS*. **C)** Quantification of polyphosphate across embryonic stages. n=75 in each time point, N=3. **D)** Quantification of polyP across a fly life cycle;- embryos (n=75, N=8), first instar larvae (n=25, N=5), second instar larvae (n=25, N=5), feeding third instar larvae (n=10, N=5), non-feeding third instar larvae (n=10, N=5), prepupae (n=20, N=3), one-days-post-pupariation pupae (n=20, N=8), pharate (n=10, N=5), three-days-post-eclosion adult (n=10, N=5). Statistics: Student's *t*-test with $p > 0.001$, error bar - s.e.m. *Drosophila* strain used - *CantonS*.

Fig 2: Validation of PPBD as a probe for polyphosphates in fly tissues A) Schematic of PolyP detection using PPBD fused at the N-terminus with a GST tag. **B)** PPBD and $PPBD^{Mut}$ predicted structural models using ColabFold v1.5.5: AlphaFold2 using MMseqs2 (free online). The amino residues marked in red are changed to Alanine (marked in orange). Overall alignment shows a r.m.s.d. Value of 0.024. **C)** Binding characteristic of GST, GST-PPBD, and GST-$PPBD^{Mut}$ with $polyP_{100}$-2X-FITC using MST. Graph showing GST-PPBD fraction bound to polyP, whereas the GST-$PPBD^{Mut}$ and GST does not bind to $polyP_{100}$-2X-FITC. **D)** Staining of hemocytes with GST, GST-PPBD, and GST-$PPBD^{Mut}$. Hml-GAL4>UAS GFP reporter was used to identify plasmocytes. Negative control cells incubated with GST and GST-PPBD Mutant proteins separately and stained with anti-GST antibody (GST; orange hot). For polyP staining, cells were incubated with GST-PPBD protein and stained with anti-GST antibody (GST-PPBD-polyphosphate; orange hot). Scale bar - 5µm. **E)** Staining of hemocytes with

GST-PPBD in fixed and permeabilised hemocytes with 2 hour pretreatment with buffer (control) and heat inactivated *Sc*PpX1, and active *Sc*PpX1 proteins. GST-PPBD proteins were stained with anti-GST antibody (GST-PPBD-polyphosphate; orange hot), and the cell is marked by Cell Mask Membrane staining dye (green). Scale bar - 5µm. **F)** Graph showing reduced anti-GST staining intensity in hemocytes treated with *Sc*PpX1. **G)** Graph showing reduced PPBD punctae intensity in hemocytes treated with *Sc*PpX1. Statistics: One way Annova with $p > 0.001$, error bar - s.d. *Drosophila* strain used - *CantonS*.

Fig 3: Polyphosphate staining of *Drosophila* tissues with PPBD. A-C) Staining of larval salivary glands with DAPI (nucleus; cyan) and anti-GST antibody (GST; orange hot). **A i, iii and B)** Samples incubated with GST (negative control). **A ii, iv and C)** Samples incubated with GST-PPBD. **B-C)** Salivary gland stained with DAPI (cyan) anti-fibrillarin antibody (magenta) and anti-GST antibody (orange hot) to detect polyphosphate colocalization within the nucleolus. Scale bar for (A i,ii,B-C)- 20µm, scale bar for (A iii,iv) - 5µm. *Drosophila* strain used - *CantonS*. **D)** Staining of fly ovaries. Negative control: Incubated with GST and stained with DAPI (nucleus; cyan) and anti-GST antibody (GST; orange hot). Stages covered - S1-S8. Incubated with GST-PPBD and stained with DAPI (nucleus; cyan) and anti-GST antibody (GST-PPBD-polyphosphate; orange hot). Stages covered - S1-S9. Yellow arrow- follicle cells, Orange arrow- nurse cells. Scale bar - 20µm. Insets reveal the nucleus and part of the cytoplasm across stages S4-S9, showing reduced polyphosphate signals. Scale bar - 5µm. *Drosophila* strain used - *CantonS*. **E-H)** GST-PPBD staining of hemocytes. *Hml-GAL4>UAS GFP* reporter was used to identify plasmocytes (E-F). *Lz-GAL4>UAS mCD8::GFP* reporter was used to identify crystal cells (G-H). Negative control (E and G) - cells incubated with GST protein and stained

with DAPI (nucleus; blue) and anti-GST antibody (GST; orange hot). For polyP staining (F and H), cells were incubated with GST-PPBD protein and stained with DAPI (nucleus; cyan) and anti-GST antibody (GST-PPBD-polyphosphate; orange hot). Scale bar of (A-D) - 5µm.

Fig 4: FLYX- Transgenic fly lines with polyP depletion expressing *Sc*PpX1. A) Schematic of creation of FLYX by cloning *S.cerevisiae ScPpX1* cDNA into pUAST-attB vector suitable for expression in flies, followed by injection into embryos. **B)** Schematic of *Drosophila* UAS-GAL4-based protein expression system. **C)** Schematic of different FLYX lines of the FLYX library- CytoFLYX, Nuc-FLYX, Mito-FLYX, and ER-FLYX. **D)** PolyP quantification from third instar larvae of *tubulin-GAL4* driven control (AttP40) and Cyto-FLYX, N=10. Statistics: Student's *t*-test with $p > 0.001$, error bar - s.e.m. **E)** Localisation of HA-*Sc*PpX1 to the target organelles in different FLYX larval muscles- *DaGAL4>CytoFLYX*,stained for HA in magenta and nucleus (DAPI in green); *DaGAL4>Nuc-FLYX*, stained for HA in magenta and nucleus (DAPI in green); *DaGAL4>ER-FLYX*, stained for HA in magenta and ER (calnexin in green); *Mef2GAL4>Mito-FLYX*, stained for HA in magenta and mitochondria (ATP5A in green). Scale bar - 10µm

Fig 5: Genetic depletion of polyP shows clotting defects in flies. A-D) Clot phenotype analysis of *tubulin-GAL4* driven Cyto-FLYX (*tubulin*-FLYX). The control is *tubulin-GAL4>*AttP40. **A)** clot structure of control (AttP40) and FLYX. The scale bar is 500 pixels, and the image dimensions in pixels are 2688 x 2200. **B-D)** Quantification of relative clot fibre number density N=3 (B), clot fibre branch point number density N=3 (C) and clot fibre length, N=4(D) of FLYX line with respect to control. Statistics: Student's *t*-test with $p > 0.001$, error bar - s.e.m. **E-P)**

Analysis of clot fibre number, branching and length phenotype upon FLYX driven by *cg-GAL4 (E-H)*, *hml*-GAL4 (I-L) and *lz*-GAL4 (M-P) with respect to control (GAL4>AttP40). Scale bar- 500 px, Image dimensions in pixels: 2688 x 2200. For quantifications - N=5. Statistics: Student's *t*-test with $p > 0.001$, error bar - s.e.m. **Q-S)** Clot phenotype of *tubulin-GAL4* driven Cyto-FLYX with exogenous Pi (Q) and $polyP_{65}$ addition (R) and quantification of fibre number density (S). Scale bar- 500 px, Image dimensions in pixels: 2688 x 2200.

Fig 6: Genetic depletion of polyP shows accelerated eclosion. A) Cumulative percentage of eclosion of control and FLYX checked after white prepupa formation (APF), m=213 (control), 268 (FLYX), N=4 (control), N=5(FLYX). **B)** Time of 50% eclosion of the control and FLYX flies- ~134 hours APF for control and 120 hours APF for FLYX, m=213 (control), 268 (FLYX), N=4 (control), N=5(FLYX). Statistics: Student's *t*-test with $p > 0.001$, error bar - s.e.m. RNA sequencing of *tubulin-GAL4* driven Cyto-FLYX (*tubulin*>FLYX) and *tubulin-GAL4*>AttP40 control third instar non-feeding wandering age matched larvae.

Fig. 1

A Schematic of polyphosphate

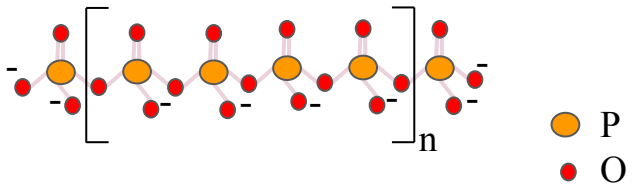

B Quantitative estimation of polyP from *Drosophila* larvae

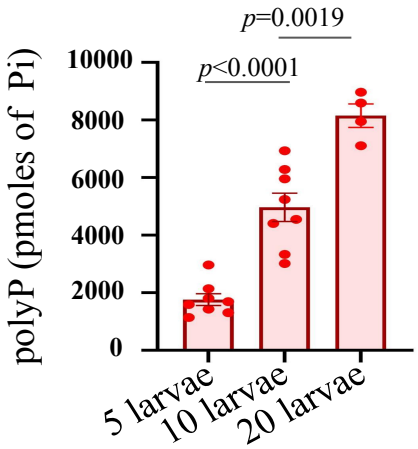

C Estimation of polyP from various embryonic stages

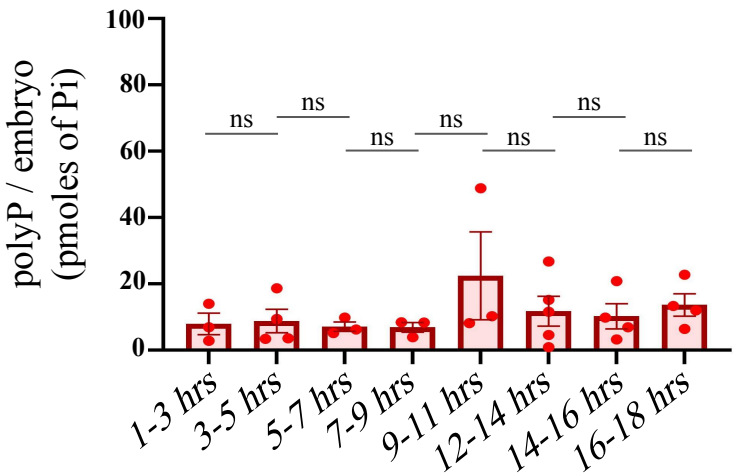

D Estimation of polyP from various life cycle stages

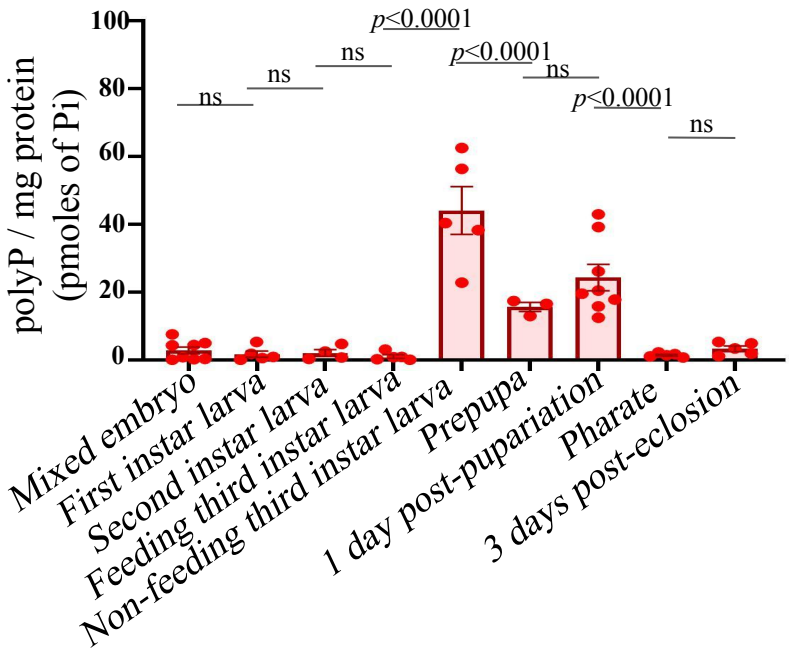

Fig 2

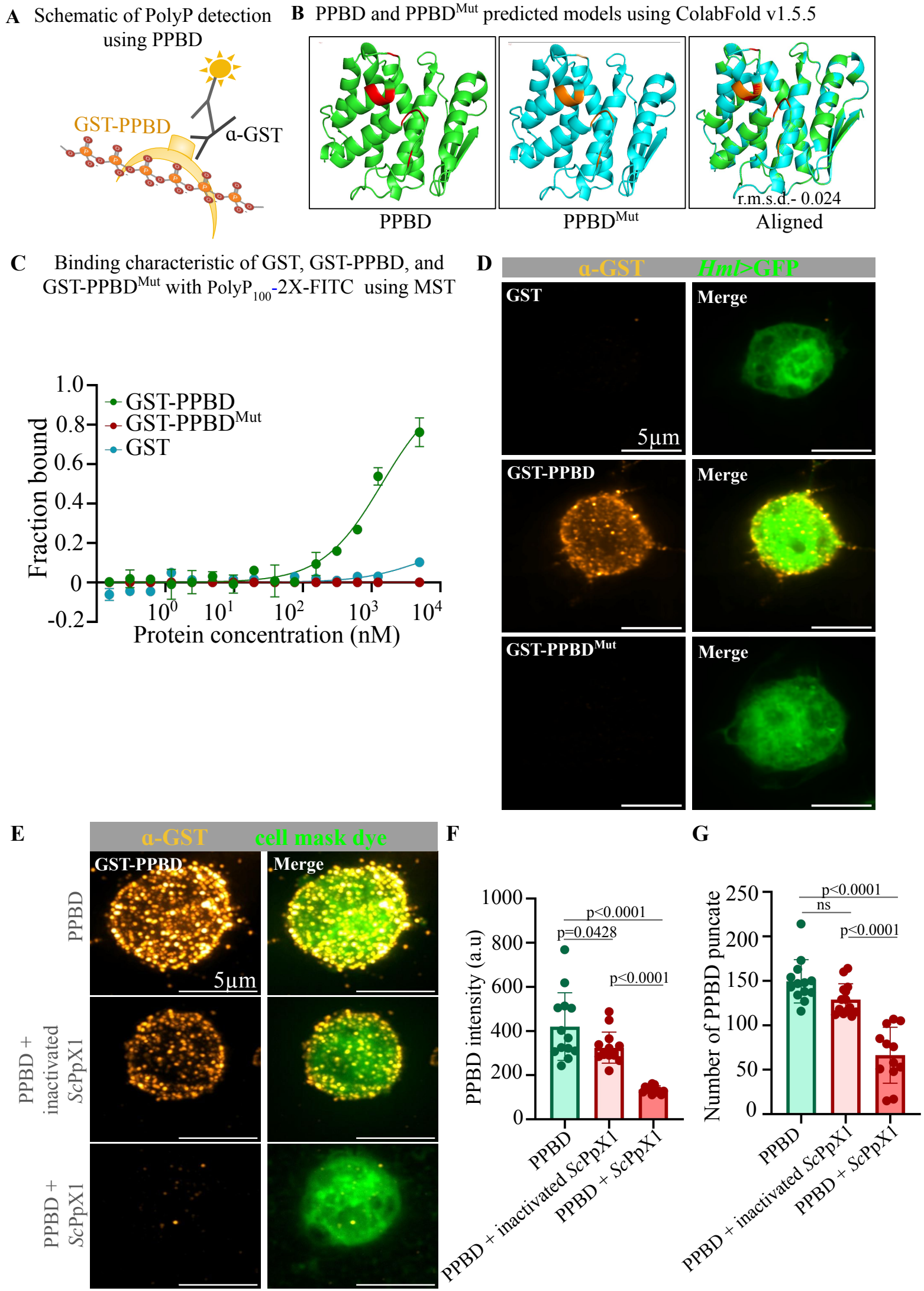
A Schematic of PolyP detection using PPBD
GST-PPBD
α-GST
B PPBD and PPBD^Mut predicted models using ColabFold v1.5.5
r.m.s.d.- 0.024
PPBD
PPBD^Mut
Aligned
C Binding characteristic of GST, GST-PPBD, and GST-PPBD^Mut with PolyP100-2X-FITC using MST
GST-PPBD
GST-PPBD^Mut
GST
Fraction bound
Protein concentration (nM)
D
α-GST
Hml>GFP
GST
Merge
5µm
GST-PPBD
GST-PPBD^Mut
E
α-GST
cell mask dye
PPBD
PPBD + inactivated ScPpX1
PPBD + ScPpX1
F
PPBD intensity (a.u)
p=0.0428
p<0.0001
G
Number of PPBD puncate
ns

Fig 3 new

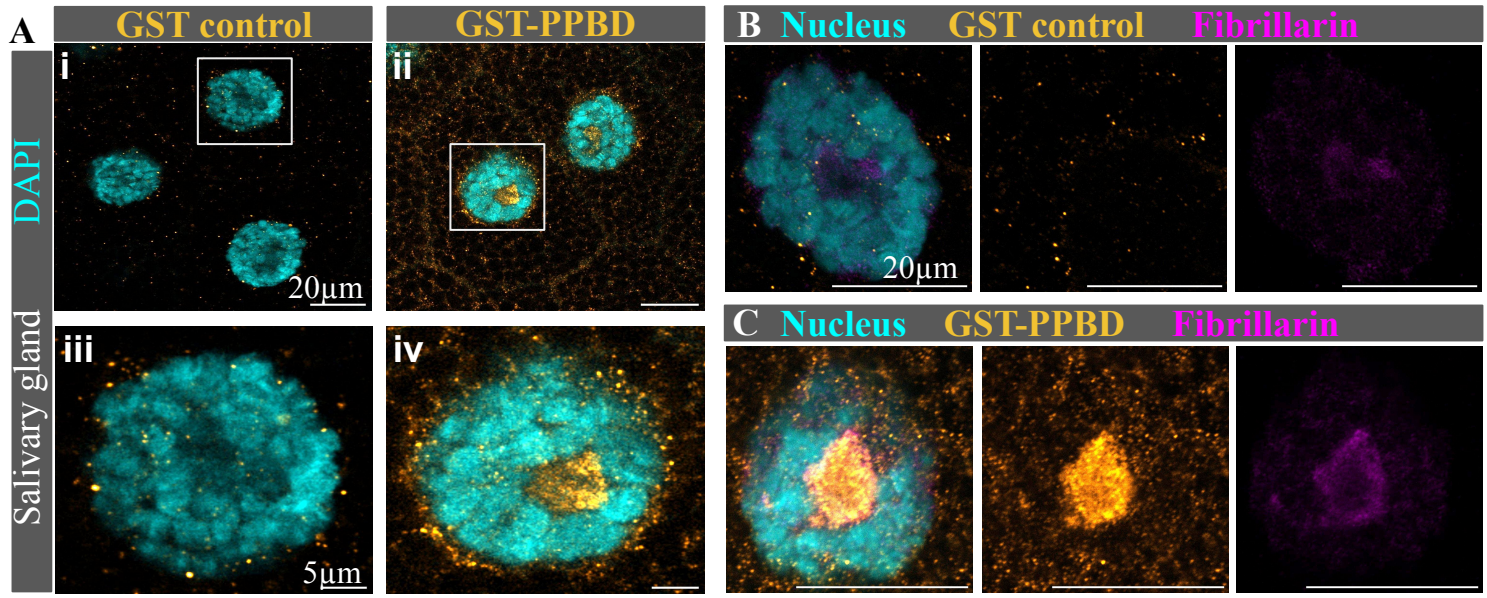
A
GST control
GST-PPBD
DAPI
Salivary gland
i
ii
iii
iv
20µm
5µm
B Nucleus GST control Fibrillarin
20µm
C Nucleus GST-PPBD Fibrillarin

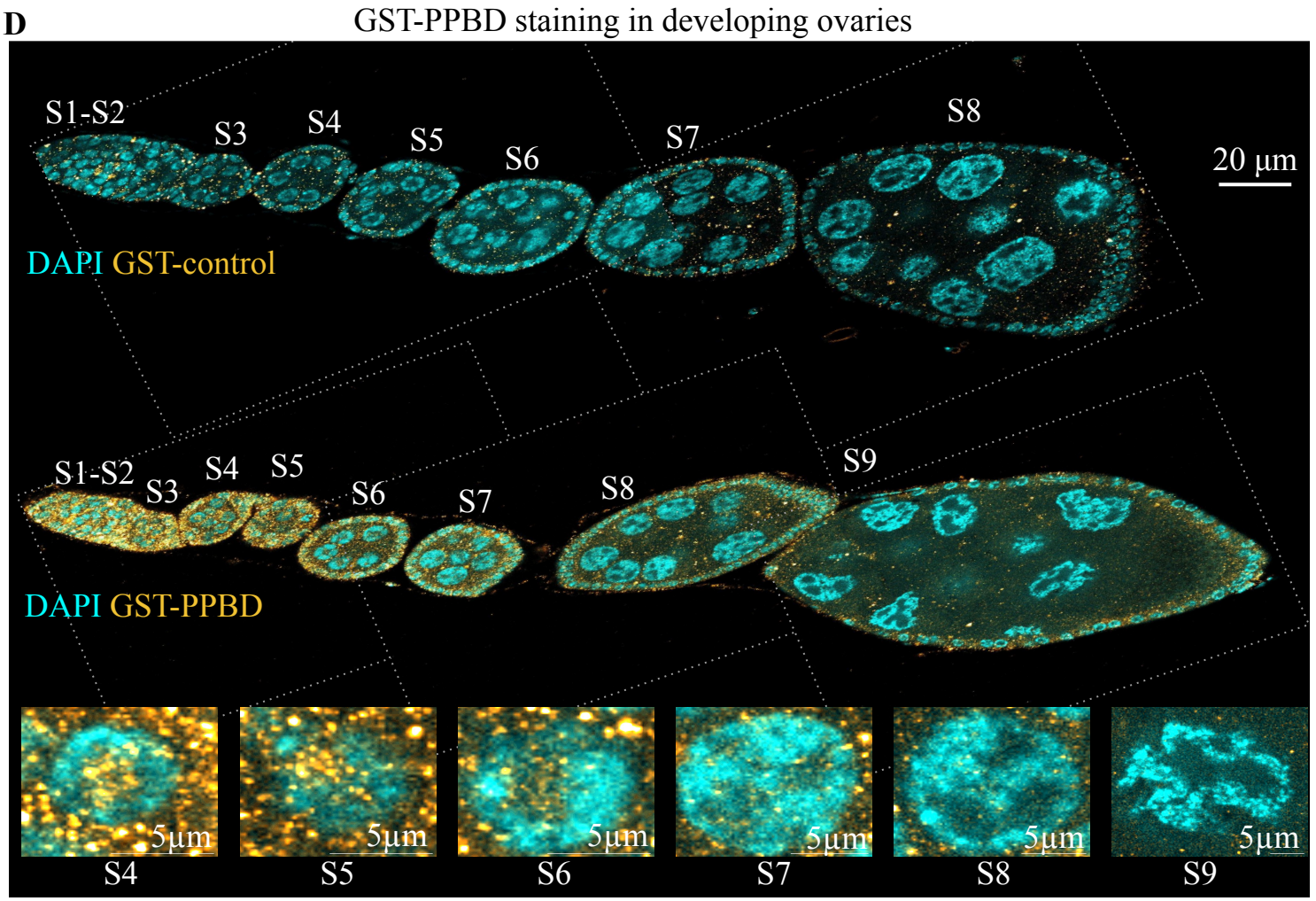
D
GST-PPBD staining in developing ovaries
S1-S2
S3
S4
S5
S6
S7
S8
S9
20 µm
DAPI GST-control
DAPI GST-PPBD
5µm
S4
S5
S6
S7
S8
S9

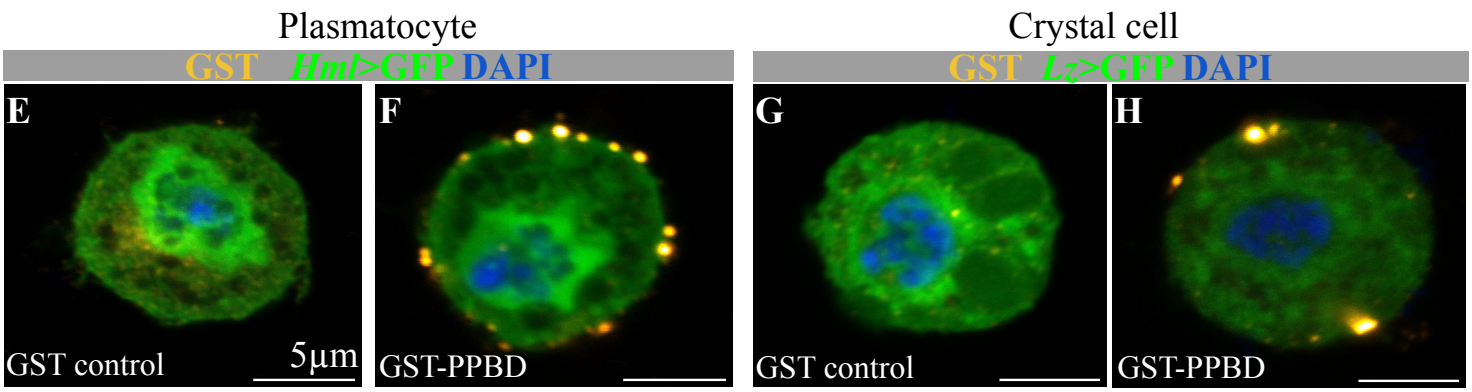
Plasmatocyte
Crystal cell
GST Hml>GFP DAPI
GST Lz>GFP DAPI
E
F
G
H
GST control
5µm
GST-PPBD
GST control
GST-PPBD

Fig 4

A fly tool for genetic polyP depletion- FLYX

A Cloning and transgenesis schematic

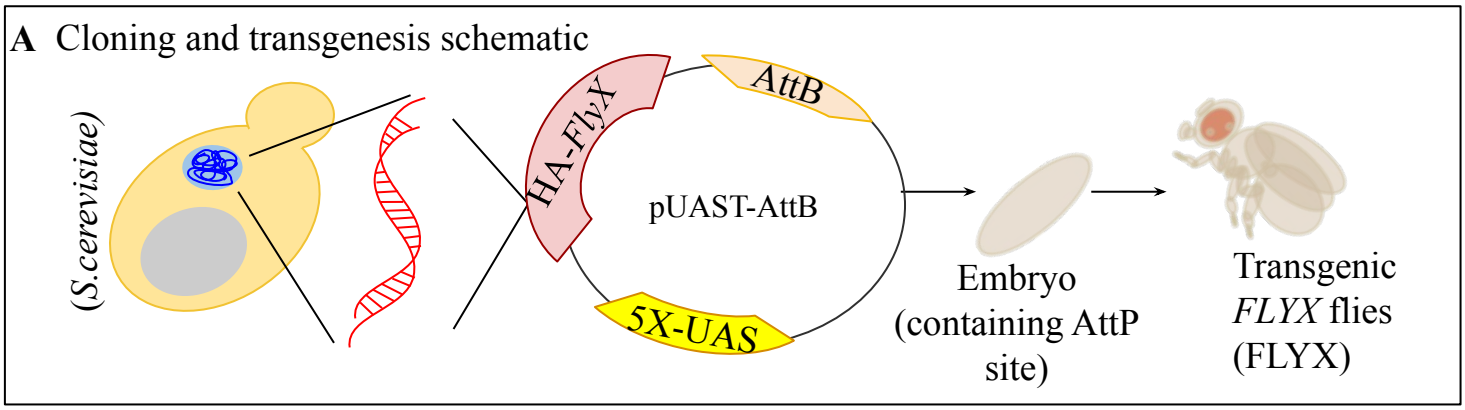

B UAS-Gal4 system to express *FLYX* in flies

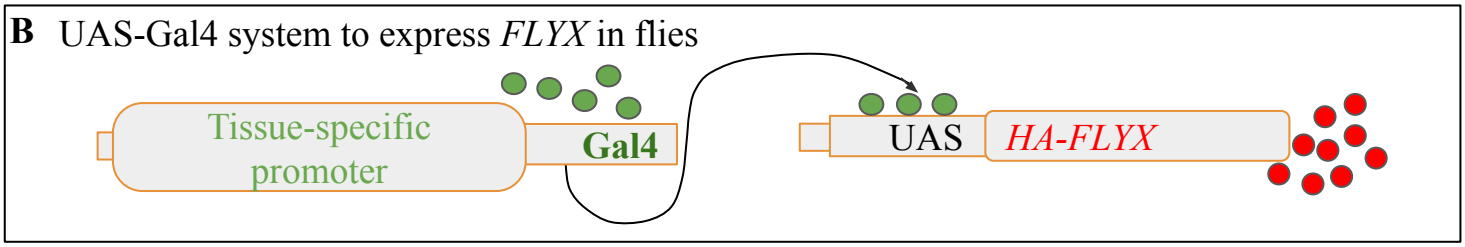

C Different FLYX construct schematic

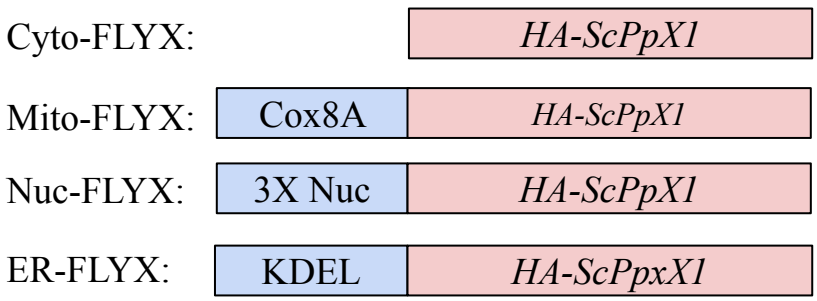

D FLYX line has functional *Sc*PpX1

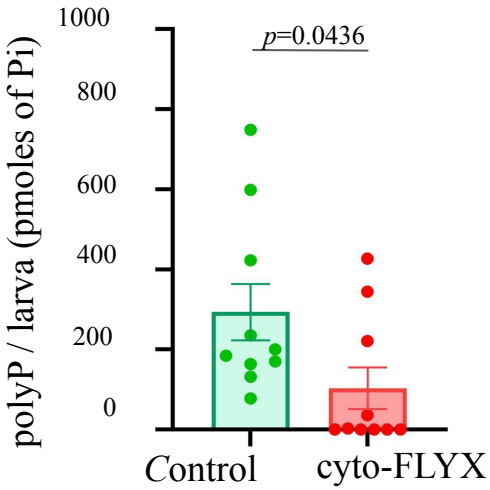

E Localisation of HA-ScPpx1 to the target organelles in different FLYX larval muscles

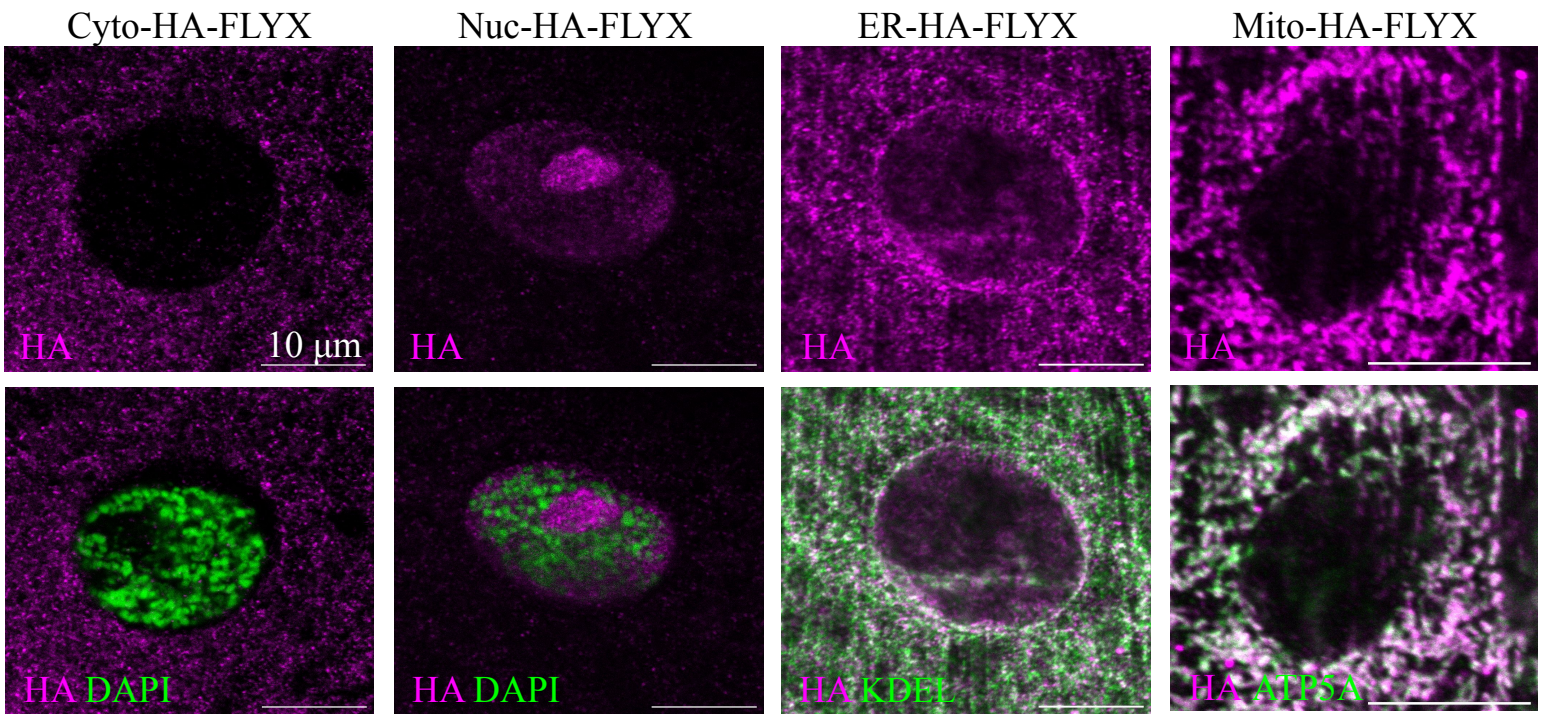

Fig 5

Cyto-FLYX show hemolymph clotting defects

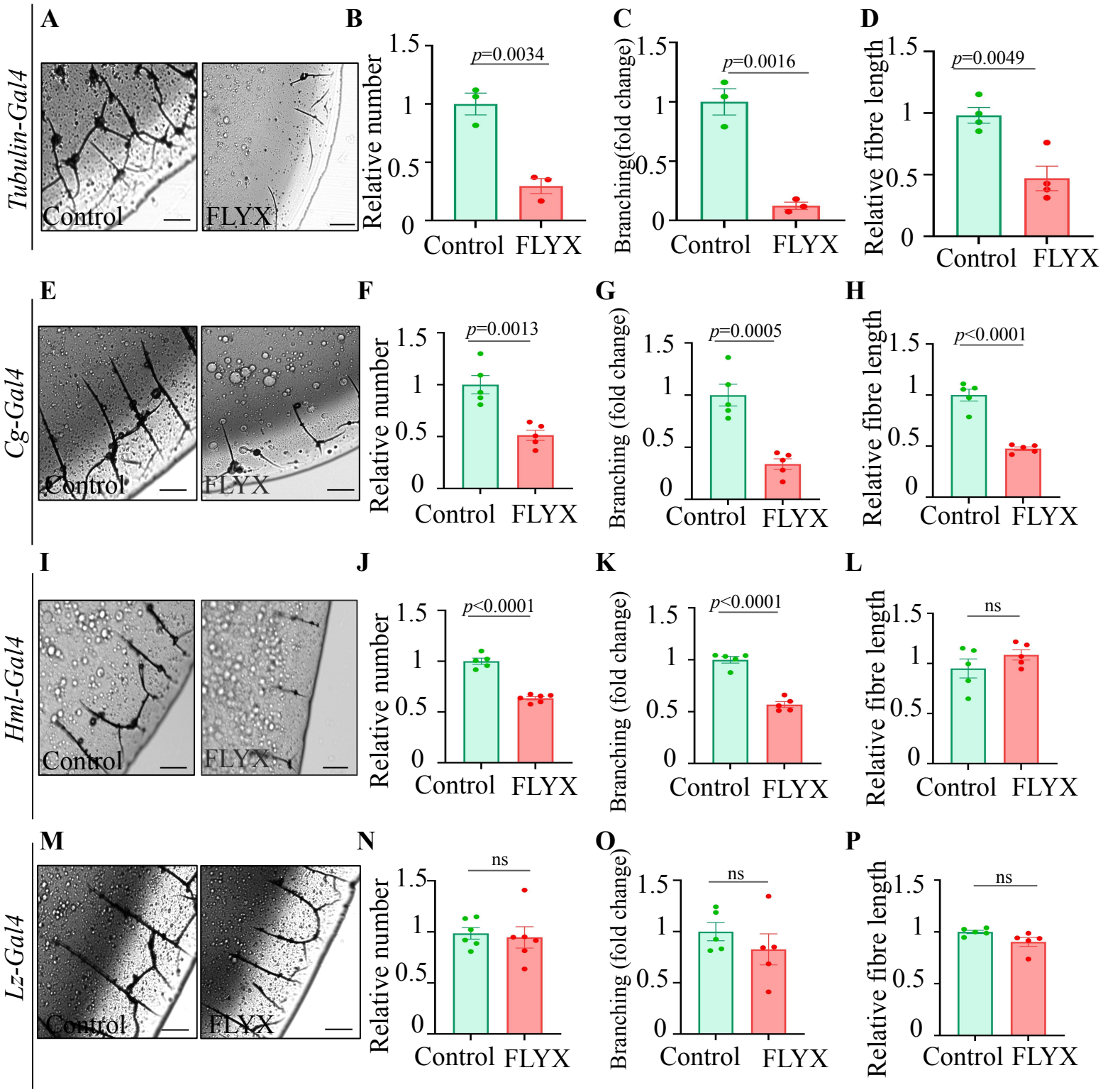

Exogenous polyP addition fail to rescue clotting defects in FLYX

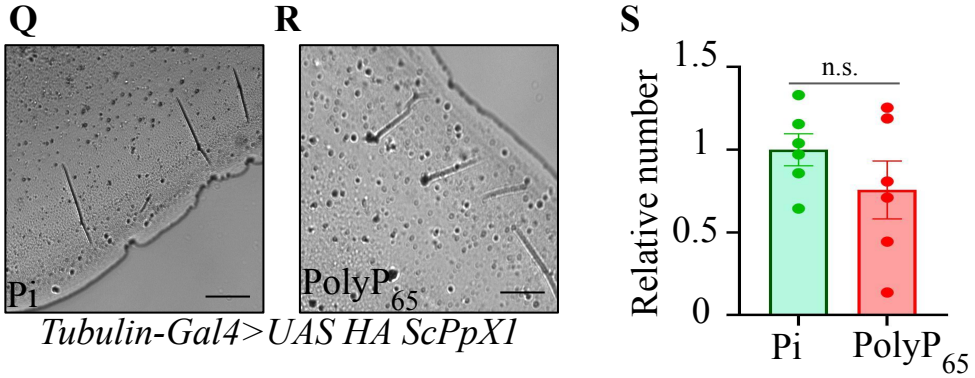

Fig 6
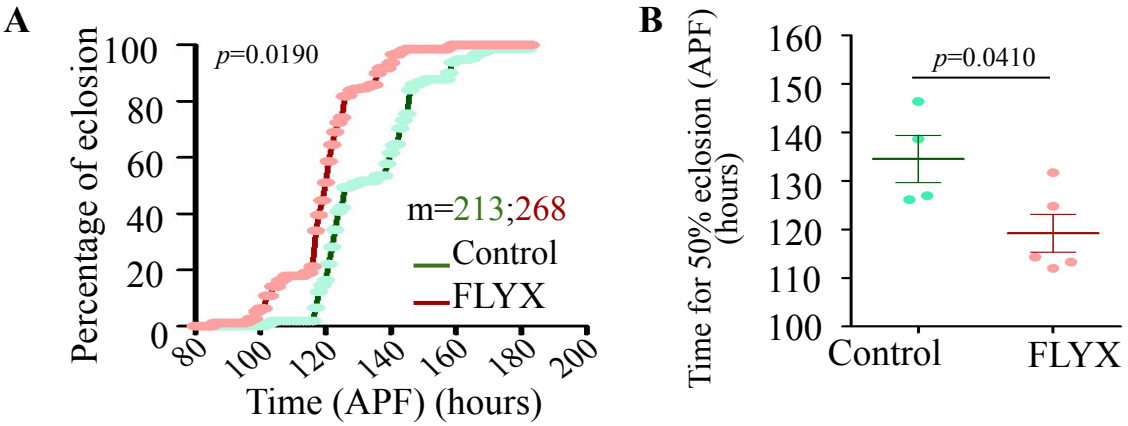
Cyto-FLYX show accelerated eclosion